

Iron and neutron-capture element abundance variations in the globular cluster M2 (NGC 7089)*

David Yong,^{1†‡} Ian U. Roederer,² Frank Grundahl,³ Gary S. Da Costa,¹ Amanda I. Karakas,¹ John E. Norris,¹ Wako Aoki,⁴ Cherie K. Fishlock,¹ A. F. Marino,¹ A. P. Milone¹ and Luke J. Shingles¹.

¹Research School of Astronomy and Astrophysics, Australian National University, Canberra, ACT 2611, Australia

²Department of Astronomy, University of Michigan, 500 Church Street, Ann Arbor, MI 48109, USA

³Stellar Astrophysics Centre, Department of Physics and Astronomy, Aarhus University, Ny Munkegade 120, DK-8000 Aarhus C, Denmark

⁴National Astronomical Observatory, Mitaka, Tokyo 181-8588, Japan

9 October 2018

ABSTRACT

We present CN and CH indices and Ca II triplet metallicities for 34 giant stars and chemical abundances for 33 elements in 14 giants in the globular cluster M2. Assuming the program stars are cluster members, our analysis reveals (*i*) an extreme variation in CN and CH line strengths, (*ii*) a metallicity dispersion with a dominant peak at $[\text{Fe}/\text{H}] \approx -1.7$ and smaller peaks at -1.5 and -1.0 , (*iii*) star-to-star abundance variations and correlations for the light elements O, Na, Al and Si and (*iv*) a large (and possibly bimodal) distribution in the abundances of all elements produced mainly via the *s*-process in solar system material. Following Roederer et al. (2011), we define two groups of stars, “*r* + *s*” and “*r*-only”, and subtract the average abundances of the latter from the former group to obtain a “*s*-process residual”. This *s*-process residual is remarkably similar to that found in M22 and in M4 despite the range in metallicity covered by these three systems. With recent studies identifying a double subgiant branch in M2 and a dispersion in Sr and Ba abundances, our spectroscopic analysis confirms that this globular cluster has experienced a complex formation history with similarities to M22, NGC 1851 and ω Centauri.

Key words: Stars: abundances – Galaxy: abundances – globular clusters: individual: NGC 7089

1 INTRODUCTION

Photometric studies have revealed complex structure in the colour-magnitude diagrams (CMD) of Galactic globular clusters (e.g., see review by Piotto 2009). The subgiant branch region is of particular interest because differences in the luminosity of stars at this evolutionary stage require distinct ages and/or chemical compositions. Any globular cluster that exhibits a broadened or split subgiant branch must therefore have experienced a complex, and likely prolonged, chemical enrichment history when compared to globular clusters with a single subgiant branch population.

ω Centauri and M22 (NGC 6656) are two Galactic globular clusters with multiple subgiant branches (e.g., Bedin et al. 2004; Marino et al. 2009). These two clusters are also notable for exhibiting a large star-to-star dispersion in the abundance of Fe-peak and neutron-capture elements (e.g., Norris & Da Costa 1995a; Smith et al. 2000; Marino et al. 2009, 2011; Johnson & Pilachowski 2010; Roederer et al. 2011). NGC 1851 is another globular cluster with multiple subgiant branches (Milone et al. 2008). Although the difference in metallicity between the two populations, $\Delta[\text{Fe}/\text{H}] \approx 0.07$ dex (Carretta et al. 2010c), is less pronounced in NGC 1851 compared to ω Cen and M22, a large star-to-star dispersion in the neutron-capture element abundances is also present (e.g., Yong & Grundahl 2008; Villanova et al. 2009; Carretta et al. 2011). While theoretical studies indicate that multiple population globular clusters could be formed through mergers or that some may be the remnants of dwarf galaxies (e.g., Bekki & Freeman

* Based in part on data collected at Subaru Telescope, which is operated by the National Astronomical Observatory of Japan. This paper includes data gathered with the 6.5 meter Magellan Telescopes located at Las Campanas Observatory, Chile.

† E-mail: david.yong@anu.edu.au

‡ Stromlo Fellow

2003; Carretta et al. 2010b; Bekki 2011; Bekki & Yong 2012), understanding the sequence of events that produce multiple population globular clusters remains a major challenge (e.g., Marcolini et al. 2007; D’Ercole et al. 2008; D’Antona et al. 2010; Conroy & Spergel 2011; Herwig et al. 2012; Vesperini et al. 2013). An important step in advancing our knowledge of the formation of multiple population globular clusters is to understand the full range of phenomena and relative frequency present in the Galactic globular cluster system.

Piotto et al. (2012) identified five new Galactic globular clusters with broadened or split subgiant branches based on *Hubble Space Telescope* photometry. Their sample included M2 (NGC 7089), a little-studied cluster. Smith & Mateo (1990) measured the strengths of the CN and CH molecular features in a sample of 19 M2 red giants. In addition to the usual bimodal distribution of CN band strengths (Smith 1987), they noted that two objects are CH stars. CH stars are rare in globular clusters, and at the time of that paper, the only other clusters known to contain CH stars included the apparently normal cluster M55 as well as the peculiar systems M22 and ω Cen. Smolinski et al. (2011) studied the CN and CH bands from Sloan Digital Sky Survey spectroscopy in a number of globular clusters including M2. They did not identify any stars with unusually strong CN or CH in this cluster, and all of their program stars lie on the canonical red giant branch (RGB). Lardo et al. (2012) studied the CN and CH band strengths as well as the C and N abundances in a sample of 35 M2 red giants. They also noted the presence of an additional RGB in the V versus $U - V$ CMD. Both CH stars identified by Smith & Mateo (1990) are located on the anomalous RGB (see Figure 14 in Lardo et al. 2012). Examination of the Grundahl et al. (1999) Strömgren photometry also confirms the peculiar nature of the RGB. While Lardo et al. (2012) did not observe any stars on the anomalous RGB, in a subsequent study they obtained spectra for such stars (Lardo et al. 2013). Stars belonging to the two RGBs had distinct C, N, Sr and Ba abundances and Lardo et al. (2013) argued that M2 has experienced a complex star formation history with similarities to ω Cen, M22 and NGC 1851.

High-resolution spectroscopy and chemical abundance measurements for a larger suite of elements for stars on the canonical and anomalous RGBs of M2 are essential to reveal the true nature of this multiple population globular cluster. The purpose of this paper is to measure CN and CH indices and chemical abundances for a sample of stars in M2 belonging to the canonical and anomalous RGBs. The sample selection and observations are described in Section 2. Section 3 contains the analysis. The results are presented in Section 4. Section 5 includes a discussion on the nature of this cluster.

2 SAMPLE SELECTION AND OBSERVATIONS

The program stars were selected from the *wby* Strömgren photometry by Grundahl et al. (1999). In Figure 1, we present the $u - y$, $v - y$, and $b - y$ CMDs. As noted by Lardo et al. (2012), we confirm the presence of an additional RGB sequence. Such stars are highlighted in red and aqua in Figure 1 and were selected from the v versus $u - y$ CMD

(upper panel in Figure 1). We refer to these as anomalous RGB stars. (The reason for using two sets of colours for the anomalous RGB stars will become clear when we present the chemical abundances for these objects: the red symbols are stars with $[\text{Fe}/\text{H}] \approx -1.5$ and the aqua symbols are stars with $[\text{Fe}/\text{H}] \approx -1.0$.) While Lardo et al. (2012) showed that the two CH stars identified by Smith & Mateo (1990) were located on the anomalous giant branch, neither was included in the Grundahl et al. (1999) photometry.

2.1 Medium-resolution spectroscopic observations

We observed candidate M2 members using the AAOmega multi-object spectrograph (Saunders et al. 2004) on the Anglo-Australian Telescope as part of two separate observing runs. The two CH stars from Smith & Mateo (1990) were also observed. The first set of observations, obtained on 2010 September 30, used the 1700B blue and 2000R red gratings. These provide spectral coverage of 3750 Å to 4440 Å and 5800 Å to 6300 Å at resolutions $R = \lambda/\Delta\lambda = 3500$ and 8000 for the red and blue arms, respectively. The second set of observations, from 2011 November 1, employed the 580V blue and 1700D red gratings. These gratings provide a wavelength coverage from 3750 Å to 5500 Å at a resolution of 1300 in the blue arm, and 8350 Å to 8825 Å at $R = 10000$ in the red arm. In each case the cluster observations were obtained together with flat-field and arc lamp calibration exposures. Data reduction to wavelength-calibrated sky-subtracted individual stellar spectra was accomplished using the standard 2DFDR¹ software. In generating the fibre configurations for the observations, high priority was given to the stars that lie on the anomalous giant branch.

Although the same input catalogue was used for both sets of observations, the combination of different field plates and different available fibre numbers meant that the two sets of stars observed are not identical. The first set contains 22 stars, the second 23 with 11 in common for a total sample of 34 candidate M2 members. The stars observed are listed in Table 1. We note that 14 stars belong to the anomalous RGB and the two CH stars from Smith & Mateo (1990) may also be regarded as anomalous RGB objects (Lardo et al. 2012, 2013). Based on their CMD location, we offer some comments on a handful of the stars observed with AAOmega. Star NR 82, if a cluster member, would be classified as a asymptotic giant branch (AGB) star rather than a RGB star. Star NR 184, if a cluster member, would be a UV-bright object lying more than a magnitude above the cluster blue horizontal branch. Similarly, star NR 648 has the photometric colours and magnitude of a cluster blue horizontal branch star. However, the AAOmega spectra (from the second data set) are that of a cluster-like red giant star. We have no straightforward explanation for this anomaly. Star NR 707, again if it is a cluster member, has a magnitude and colour that would suggest it is a red horizontal branch (RHB) star. M2, however, is not normally considered to have a RHB population given its dominant blue HB morphology (e.g., Lardo et al. 2012). We have not considered these stars any further in the analysis.

¹ http://www.aao.gov.au/2df/aaomega/aaomega_2dfdr.html

Table 1. Program stars observed with AAOmega.

Name1 ^a (1)	Name2 (2)	RA. 2000 (3)	Dec. 2000 (4)	P(%) ^b (5)	Flag ^c (6)	V (7)	RV (km s ⁻¹) (8)	σ RV (km s ⁻¹) (9)	S(3839) (10)	m_{CH} (11)
2010 09 30										
HI-240	AIII-43	21 33 10.70	-00 51 09.67	99	...	14.25	1.6	2.0	1.183	0.082
HI-451	...	21 33 39.11	-00 49 30.18	15.86	2.1	4.6	0.574	0.150
NR 38	...	21 33 28.91	-00 50 00.94	...	1	13.60	1.1	2.2	0.520	0.045
NR 76	HI-104,AII-30	21 33 17.91	-00 48 19.82	99	...	13.85	-1.5	4.9	0.291	0.049
NR 81	...	21 33 27.08	-00 48 19.41	...	1	13.81	-16.8	2.2	0.350	0.157
NR 124	...	21 33 27.81	-00 47 30.43	14.21	4.3	2.3	0.421	0.009
NR 132	...	21 33 23.10	-00 48 11.53	...	1	14.20	0.8	2.5	0.245	0.023
NR 184 ^d	CR57	21 33 24.94	-00 50 41.42	99	...	15.24	0.0	7.8	0.002	-0.113
NR 216	CR19	21 33 31.48	-00 49 06.33	99	1	14.82	-12.1	2.7	0.652	0.038
NR 225	HI-586,AI-58	21 33 29.27	-00 45 55.49	99	...	14.82	-10.6	5.2	0.492	0.025
NR 301	AIV-37	21 33 32.80	-00 50 27.06	99	1	14.93	-6.3	3.2	0.693	0.098
NR 358	HI-521,AI-79	21 33 34.05	-00 47 32.10	99	1	15.06	-16.0	4.2	1.459	0.043
NR 378	AI-50	21 33 30.32	-00 47 24.54	99	1	15.22	3.2	5.2	0.363	0.086
NR 386	...	21 33 26.18	-00 49 21.35	...	1	15.70	-3.4	3.7	0.057	-0.061
NR 388	...	21 33 27.16	-00 50 25.43	15.23	-6.0	6.0	0.293	-0.022
NR 417	CR76	21 33 23.48	-00 48 46.57	99	...	15.39	-2.9	3.3	0.212	0.017
NR 721	...	21 33 24.32	-00 49 41.46	...	1	15.79	-8.8	1.8	0.309	0.002
NR 811	...	21 33 22.85	-00 50 34.00	15.74	-9.3	5.2	0.388	0.013
NR 847	...	21 33 23.45	-00 46 24.34	15.79	-16.1	2.8	0.430	-0.008
NR 915	...	21 33 35.36	-00 49 57.45	15.83	-5.2	6.9	0.319	0.037
NR 1178	...	21 33 31.64	-00 49 59.80	...	1	16.06	3.0	5.1	0.343	0.059
NR 1204	AIII-26	21 33 20.08	-00 50 13.76	99	1	15.82	-7.9	3.3	0.561	0.154
2011 11 01										
HI-240	AIII-43	21 33 10.70	-00 51 09.67	99	...	14.25	2.9	2.5	1.069	0.085
HI-451	...	21 33 39.11	-00 49 30.18	15.86	4.3	2.7	0.609	0.199
NR 47	CR12	21 33 28.52	-00 48 43.92	99	1	13.70	5.1	1.5	0.483	0.058
NR 76	HI-104,AII-30	21 33 17.91	-00 48 19.82	99	...	13.85	-1.5	1.9	0.283	0.045
NR 82 ^d	CR190	21 33 33.63	-00 50 29.50	99	...	13.91	-3.1	1.7	0.424	-0.015
NR 99	AIII-86	21 33 23.59	-00 50 41.07	99	...	13.69	-1.3	2.1	0.250	0.018
NR 124	...	21 33 27.81	-00 47 30.43	14.21	4.4	1.9	0.382	0.017
NR 132	...	21 33 23.10	-00 48 11.53	...	1	14.20	1.2	2.2	0.337	0.053
NR 207	...	21 33 27.48	-00 49 51.35	...	1	14.89	-1.1	2.0	0.219	0.004
NR 225	HI-586,AI-58	21 33 29.27	-00 45 55.49	99	...	14.82	-10.8	2.0	0.430	0.049
NR 254	...	21 33 29.37	-00 49 42.84	...	1	15.05	3.4	2.0	0.255	0.027
NR 299	AI-22	21 33 35.32	-00 49 22.13	99	...	14.94	0.3	1.9	0.307	0.120
NR 358	HI-521,AI-79	21 33 34.05	-00 47 32.10	99	1	15.06	-16.7	1.2	1.328	0.114
NR 375	...	21 33 30.62	-00 50 08.33	15.20	2.1	1.7	0.322	0.022
NR 378	AI-50	21 33 30.32	-00 47 24.54	99	1	15.22	-2.3	2.0	0.432	0.081
NR 403	CR58	21 33 25.64	-00 50 43.12	99	...	15.20	-15.3	1.8	0.331	0.015
NR 648 ^d	...	21 33 26.32	-00 49 10.58	15.99	-1.6	1.9	0.194	-0.049
NR 707 ^d	...	21 33 23.02	-00 48 56.69	15.81	0.3	1.9	0.095	-0.053
NR 801	...	21 33 27.46	-00 46 53.10	15.79	-2.3	2.2	0.305	-0.004
NR 847	...	21 33 23.45	-00 46 24.34	15.79	-3.9	2.0	0.377	0.034
NR 915	...	21 33 35.36	-00 49 57.45	15.83	-11.8	2.3	0.332	0.047
NR 947	AIII-10	21 33 18.75	-00 49 44.09	99	...	15.79	-6.2	1.9	0.190	0.059
NR 1204	AIII-26	21 33 20.08	-00 50 13.76	99	1	15.82	-10.6	1.7	0.449	0.123

^a AXXX names are from Arp (1955), CRXXX names are from Cudworth & Rauscher (1987), HXXX names are from Harris (1975), and NR XXX names are from the Grundahl et al. (1999) photometry.

^b Probability of cluster membership from Cudworth & Rauscher (1987).

^c 1 = stars which lie on the anomalous giant branch selected from the v versus $u - y$ CMD. All other stars lie on the canonical RGB.

^d NR 184 is a UV-bright star, NR 648 is a BHB star, NR 707 is a RHB (or AGB) star and NR 82 is an AGB star.

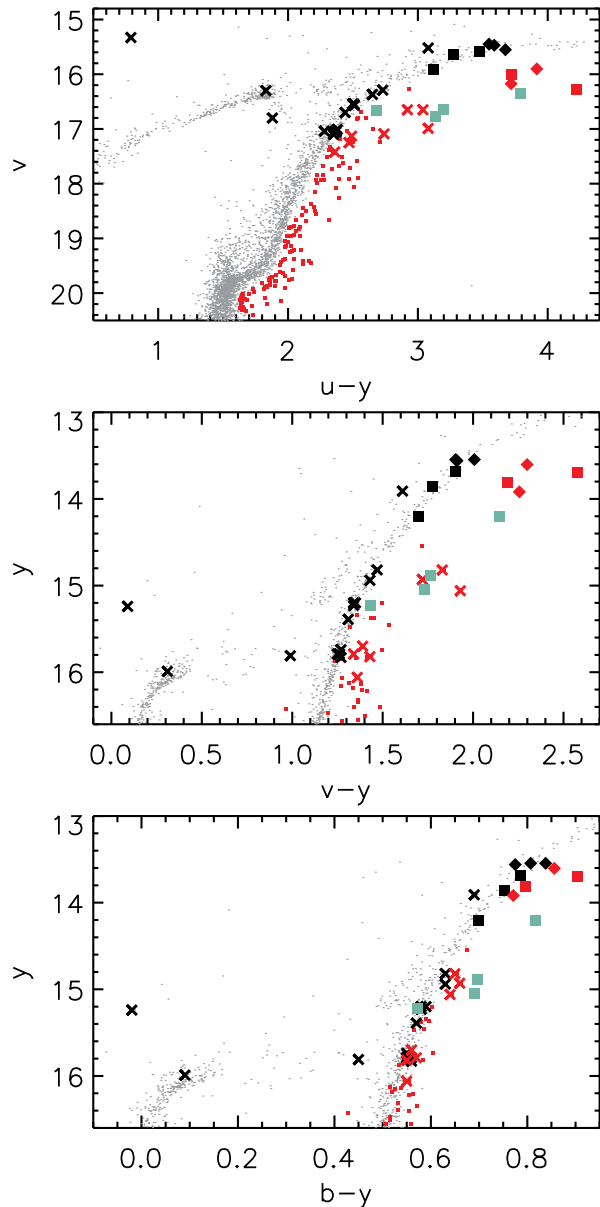


Figure 1. Colour-magnitude diagrams for v versus $u - y$ (upper), y versus $v - y$ (middle) and y versus $b - y$ (lower). The black symbols are stars that lie on the canonical RGB, AGB or HB as well as one UV bright object. The red (and aqua) symbols are stars that lie on the anomalous RGB, and were selected from the v versus $u - y$ CMD, upper panel. (The aqua symbols are the unusually metal-rich objects as determined from high-resolution spectroscopy.) Crosses represent stars observed with the AAT. Square symbols (Subaru Telescope) and diamond symbols (Magellan Telescope) represent objects observed at high spectral resolution.

2.2 High-resolution spectroscopic observations

Three stars (NR 76, NR 81 and NR 132) were observed in service mode using the High Dispersion Spectrograph (HDS, Noguchi et al. 2002) on the Subaru Telescope on 2011 August 3. Six additional stars (NR 47, NR 99, NR 124, NR 207, NR 254 and NR 378) were observed using HDS in classical mode on 2013 July 17. All nine stars were also observed with

the AAOmega instrument. For both sets of observations, we used the StdYb setting and the $0''.8$ slit which resulted in a wavelength coverage from $\sim 4100 \text{ \AA}$ to $\sim 6800 \text{ \AA}$ at a spectral resolution of $R = 45000$. A telluric standard was also observed. The spectra were reduced using IRAF² adopting a similar approach as in Yong et al. (2006).

Five stars (NR 37, NR 38, NR 58, NR 60 and NR 77) were also observed using the Magellan Inamori Kyocera Echelle (MIKE) spectrograph (Bernstein et al. 2003) at the Magellan Telescope on 2012 August 26. NR 60 is a likely AGB star based on CMD location. Full wavelength coverage was obtained ($\sim 3400 \text{ \AA}$ to $\sim 9000 \text{ \AA}$), and we used the $0''.7$ slit which provided a spectral resolution of $R = 40000$ in the blue arm and $R = 35000$ in the red arm, as measured from the ThAr lines. The spectra were reduced using the CARPY pipeline³ and independently in IRAF using the MTOOLS package⁴. One star, NR 77, had a faint, nearby companion. This object was reduced in two different ways using IRAF. In the first approach, we adopted a conservative aperture placement to try to avoid flux from the faint companion. In the second approach, the flux from both stars was extracted. In the subsequent section, we analyze both sets of spectra independently in order to quantify the contamination from the nearby companion. The program stars are listed in Table 2. We note that of these 14 objects observed at high spectral resolution, six belong to the canonical RGB and eight are anomalous RGB stars.

In Figures 2 to 5, we plot regions of the high dispersion spectra for the program stars from both telescope+instrument combinations. These figures demonstrate that there are star-to-star variations in the strengths of Zr and La lines which could be caused by differences in stellar parameters and/or chemical abundance ratios. In Section 3.2, we shall seek to quantify the stellar parameters and chemical abundances.

3 ANALYSIS

3.1 Radial velocities and line indices from medium-resolution spectra

Radial velocities were measured from the medium-resolution spectra by cross-correlating each program star against HI-240. The radial velocity for HI-240 was determined by measuring the wavelengths of a small set of lines (sodium doublet 5889.951 \AA and 5895.924 \AA and the calcium triplet 8498.03 \AA , 8542.09 \AA and 8662.14 \AA). Given the superior spectral resolution in the red arm, we adopted those values as the radial velocities and corrected for the heliocentric motion. We measured the $S(3839)$ and m_{CH} indices in the AAOmega spectra using the definitions given in Smith & Mateo (1990). Calcium triplet line strengths were measured via Gaussian line profile fits to the observed data for the two stronger Ca II triplet lines at

² IRAF is distributed by the National Optical Astronomy Observatories, which are operated by the Association of Universities for Research in Astronomy, Inc., under cooperative agreement with the National Science Foundation.

³ <http://code.obs.carnegiescience.edu/mike>

⁴ <http://www.lco.cl/telescopes-information/magellan/instruments/mike/iraf-tools/iraf-mtools-package>

Table 2. Program stars and stellar parameters for objects observed with Magellan or Subaru.

Name1 ^a	Name2	R.A.	Dec.	P ^b (%)	Flag ^c	Run ^d	V	RV (km s ⁻¹)	σRV (10)	T _{eff} (K)	log g (cgs)	ξ _t (km s ⁻¹)	[m/H] ^e (dex)	[Fe/H] (dex)
(1)	(2)	(3)	(4)	(5)	(6)	(7)	(8)	(9)	(10)	(11)	(12)	(13)	(14)	(15)
Canonical RGB (<i>r</i> -only) stars (black circles or lines in the figures)														
NR 37	CR78	21 33 25.44	-00 48 53.73	99	...	M12	13.56	-15.3	1.0	4250	0.70	1.77	-1.6	-1.66
NR 58	CR30	21 33 32.17	-00 50 01.17	99	...	M12	13.55	11.8	1.0	4225	0.70	1.89	-1.6	-1.64
NR 60 ^f	CR28	21 33 32.57	-00 49 45.72	99	...	M12	13.55	-7.1	1.0	4325	0.30	2.19	-1.7	-1.75
NR 76	HI-104	21 33 17.91	-00 48 19.82	99	...	S11	13.85	-1.3	0.6	4375	0.90	1.73	-1.7	-1.69
NR 99	AIII-86	21 33 23.59	-00 50 41.07	99	...	S13	13.69	-1.5	0.6	4275	0.70	1.78	-1.6	-1.66
NR 124	...	21 33 27.81	-00 47 30.43	S13	14.21	3.4	0.7	4425	0.85	1.81	-1.6	-1.64
Anomalous RGB (<i>r</i> + <i>s</i>) stars with [Fe/H] ≈ -1.5 (red triangles or lines in the figures)														
NR 38	...	21 33 28.91	-00 50 00.94	...	1	M12	13.60	3.7	1.3	4175	0.60	2.12	-1.6	-1.61
NR 47	CR12	21 33 28.52	-00 48 43.92	99	1	S13	13.70	3.3	0.5	4050	0.65	1.77	-1.4	-1.42
NR 77	...	21 33 24.45	-00 48 36.29	...	1	M12	13.92	6.6	1.0	4350	1.00	2.25	-1.5	-1.46
NR 81	...	21 33 27.08	-00 48 19.41	...	1	S11	13.81	-22.0	0.5	4275	1.00	1.85	-1.6	-1.55
Anomalous RGB (metal-rich) stars with [Fe/H] ≈ -1.0 (aqua star symbols or lines in the figures)														
NR 132	...	21 33 23.10	-00 48 11.53	...	1	S11	14.20	0.7	0.5	4325	1.30	1.88	-1.0	-0.97
NR 207	...	21 33 27.48	-00 49 51.35	...	1	S13	14.89	-2.1	0.4	4425	1.30	1.40	-1.1	-1.08
NR 254	...	21 33 29.37	-00 49 42.84	...	1	S13	15.05	3.2	0.5	4525	1.60	1.61	-1.0	-0.97
NR 378	AI-50	21 33 30.32	-00 47 24.54	99	1	S13	15.22	-2.9	0.5	4750	1.50	1.68	-1.1	-1.08

^a AXXX names are from Arp (1955), CRXXX names are from Cudworth & Rauscher (1987), HXXX names are from Harris (1975), and NR XXX names are from the Grundahl et al. (1999) photometry.

^b Probability of cluster membership from Cudworth & Rauscher (1987).

^c 1 = stars which lie on the anomalous giant branch selected from the *v* versus *u* - *y* CMD. All other stars lie on the canonical RGB.

^d M12 = Magellan Telescope 2012 08 26, S11 = Subaru Telescope 2011 08 03, S13 = Subaru Telescope 2013 07 17.

^e [m/H] refers to the metallicity used to generate the model atmosphere.

^f NR 60 is a likely AGB star.

8542 Å and 8662 Å using the technique first described in Armandroff & Da Costa (1991). The heliocentric radial velocities and $S(3839)$ and m_{CH} indices are presented in Table 1.

An assessment of the internal errors associated with these measurement can be obtained by consideration of the 11 objects observed on both runs. For the radial velocities, 10 of the 11 objects showed no evidence ($\leq 1\sigma$, i.e., less than one standard deviation) for radial velocity variation between the two observing runs. One star, NR 847, exhibited evidence for radial velocity variability; $-16.1 \text{ km s}^{-1} \pm 2.8 \text{ km s}^{-1}$ (2010) versus $-3.9 \text{ km s}^{-1} \pm 2.0 \text{ km s}^{-1}$ (2011). Excluding NR 847, the average difference in radial velocity for stars observed on both runs is $1.2 \text{ km s}^{-1} \pm 0.9 \text{ km s}^{-1}$ ($\sigma = 2.9 \text{ km s}^{-1}$). For the $S(3839)$ and m_{CH} indices, we find mean differences for stars observed on both runs of 0.028 ± 0.023 ($\sigma = 0.075$) and 0.018 ± 0.009 ($\sigma = 0.029$), respectively. Since for the Ca II triplet spectra only single observations are available, we adopt the uncertainty in the pseudo-equivalent widths which results from the uncertainties in the Gaussian fit parameters for the observed line profiles.

An assessment of the systematic errors can be obtained by comparison of our measurements with literature values. For the radial velocities, five of our program stars were also observed by Lardo et al. (2012, 2013), noting that on average their measurement errors ($\langle \sigma_{\text{RV}} \rangle = 16.5 \text{ km s}^{-1}$) are

larger than ours ($\langle \sigma_{\text{RV}} \rangle = 3.0 \text{ km s}^{-1}$). For three of these five stars our radial velocity measurements are in agreement. The two stars with poor agreement are NR 132, $-16.4 \text{ km s}^{-1} \pm 7 \text{ km s}^{-1}$ (Lardo et al. 2013) versus $0.9 \text{ km s}^{-1} \pm 3.4 \text{ km s}^{-1}$ (this study), and NR 378, $-60.3 \text{ km s}^{-1} \pm 5.8 \text{ km s}^{-1}$ (Lardo et al. 2013) versus $0.5 \text{ km s}^{-1} \pm 5.6 \text{ km s}^{-1}$ (this study). These stars may be spectroscopic binaries.

The $S(3839)$ and m_{CH} values are in good agreement with those of Smith & Mateo (1990) for the two stars in common. For HI-240, our mean values are $S(3839) = 1.126$ and $m_{\text{CH}} = 0.084$ and the Smith & Mateo (1990) values are 1.111 and 0.067, respectively. For HI-451, our mean values are $S(3839) = 0.592$ and $m_{\text{CH}} = 0.175$ and the Smith & Mateo (1990) values are 0.571 and 0.165, respectively. We note that the differences for $S(3839)$ and m_{CH} between this study and Smith & Mateo (1990) are comparable to mean differences for the 11 stars observed on both AAOmega runs.

3.2 Stellar parameters, chemical abundances and radial velocities from high-resolution spectra

Equivalent widths (EW) were measured from the high-resolution spectra using routines in IRAF and DAOSPEC (Stetson & Pancino 2008). When using IRAF to measure an EW, every line in every star was visually inspected. In a given star, lines regarded to be blended or poorly fit were

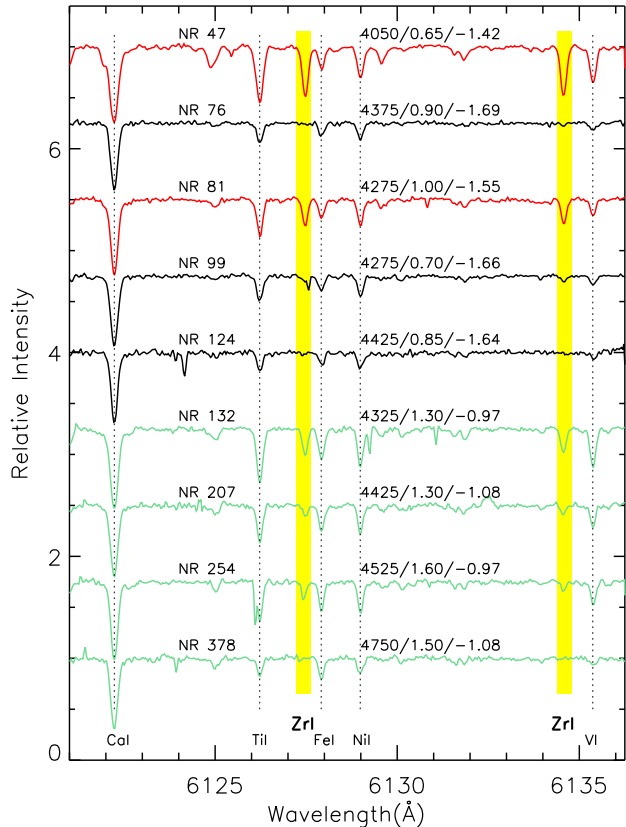


Figure 2. A portion of the Subaru HDS spectra for nine program stars. The yellow region highlights Zr I lines used in the analysis. There are clear star-to-star differences in the Zr I line strengths, and also for VI and Ti I lines. Black lines represent stars that lie on the canonical RGB. Red lines are stars on the anomalous RGB. The aqua lines are the unusually metal-rich objects on the anomalous RGB. (The colours are consistent with those used in Figure 1.) The positions of other atomic lines and the stellar parameters ($T_{\text{eff}}/\log g/[\text{Fe}/\text{H}]$) are included.

excluded, and weak ($EW < 5 \text{ m}\text{\AA}$) and strong ($EW > 130 \text{ m}\text{\AA}$) lines were also removed from the analysis. When using DAOSPEC to measure EWs, the continuum was the same as in the IRAF analysis, i.e., DAOSPEC did not re-adjust the continuum level. Additionally, the set of lines measured using DAOSPEC was identical to those already measured, and visually inspected, using IRAF. For the Subaru and Magellan spectra, there was good agreement ($\sigma = 1.5 \text{ m}\text{\AA}$) between the two sets of EW measurements, and we adopted the DAOSPEC values. For the Magellan spectra, EW measurements could be compared between the CARPY reduction and the IRAF reduction. Again, there was excellent agreement between the two sets of measurements ($\sigma = 1.4 \text{ m}\text{\AA}$). The EW measurements and line list are presented in Table 3.

To determine the stellar parameters, we adopted a traditional spectroscopic approach. We used one dimensional local thermodynamic equilibrium (LTE) model atmospheres with $[\alpha/\text{Fe}] = +0.4$ from the Castelli & Kurucz (2003) grid. To produce particular models we used the interpolation software tested in Allende Prieto et al. (2004). Chemical abundances were computed using the LTE stellar line analysis program MOOG (Snedden 1973; Sobeck et al. 2011). The ef-

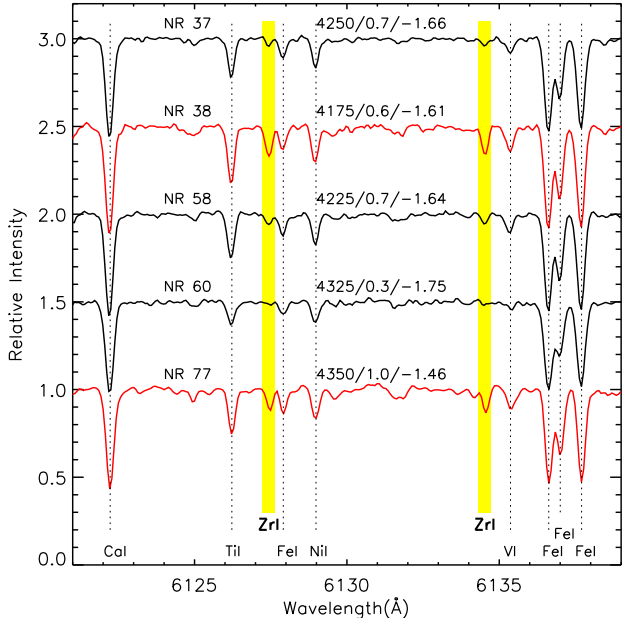


Figure 3. A portion of the Magellan MIKE spectra for five program stars. As in Figure 2, Zr lines are highlighted and there are significant star-to-star differences in line strengths. The black spectra denote that those stars lie on the canonical RGB while red spectra represent stars that lie on the anomalous RGB. The positions of other atomic lines and the stellar parameters ($T_{\text{eff}}/\log g/[\text{Fe}/\text{H}]$) are included.

fective temperature, T_{eff} , was adjusted until there was no trend between the abundance from Fe I lines and the lower excitation potential (L.E.P). The surface gravity, $\log g$, was adjusted until the abundance from Fe I lines was the same as from Fe II lines. The microturbulent velocity, ξ_t , was established when there was no trend between the abundance from Fe I and the reduced equivalent width, $EW_r = \log(EW/\lambda)$. Finally, we required that the derived metallicity was within 0.1 dex of the value adopted in the model atmosphere. The final stellar parameters (see Table 2) were obtained when these four conditions were simultaneously satisfied. We note that NR 60, whose CMD location is consistent with being an AGB star, has a surface gravity appropriate for that evolutionary phase.

Uncertainties in the stellar parameters were obtained in the following manner. For T_{eff} and ξ_t we measured the uncertainty in the slope between the abundance from Fe I lines and L.E.P. and EW_r , respectively. We then adjusted T_{eff} or ξ_t until the slope matched the relevant uncertainty. For $\log g$, we added the standard error of the mean for Fe I and Fe II in quadrature, then adjusted $\log g$ until the difference in abundances from Fe I and Fe II was equal to this value. Adopting this approach, we estimate that the internal uncertainties in T_{eff} , $\log g$ and ξ_t are 50 K, 0.2 dex and 0.2 km s^{-1} , respectively, and these are slightly conservative estimates.

For T_{eff} and $\log g$, we can compare the spectroscopic values to photometric values. For T_{eff} , we used the infrared flux method (IRFM) metallicity-dependent colour-temperature relations of Ramírez & Meléndez (2005) for giant stars. We assumed a reddening $E(B - V) = 0.06$ as in the Harris

Table 3. Line list for the program stars

Wavelength Å (1)	Species ^a (2)	L.E.P eV (3)	log <i>gf</i> (4)	NR 37 mÅ (5)	NR 38 mÅ (6)	NR 47 mÅ (7)	NR 58 mÅ (8)	NR 60 mÅ (9)	NR 76 mÅ (10)	NR 77 mÅ (11)	NR 81 mÅ (12)	Source ^b (13)
6300.31	8.0	0.00	-9.75	32.3	53.5	...	43.7	23.3	49.3	B
6363.78	8.0	0.02	-10.25	...	26.3	...	16.1	12.0	...	14.2	22.3	A
4751.82	11.0	2.10	-2.11	11.2	...	B
4982.83	11.0	2.10	-0.91	20.8	48.2	39.0	A
5682.65	11.0	2.10	-0.67	51.6	49.7	112.7	37.8	45.5	24.9	...	57.6	B

^a The digits to the left of the decimal point are the atomic number. The digit to the right of the decimal point is the ionization state (“0” = neutral, “1” = singly ionised).

^b A = log *gf* values taken from Yong et al. (2005) where the references include Den Hartog et al. (2003), Ivans et al. (2001), Kurucz & Bell (1995), Prochaska et al. (2000), Ramírez & Cohen (2002); B = Gratton et al. (2003); C = Oxford group including Blackwell et al. (1979a,b, 1980, 1986, 1995); D = Biemont et al. (1991); E1 = Fuhr & Wiese (2009), using line component patterns for hfs/IS from Kurucz & Bell (1995); E2 = Roederer & Lawler (2012); E3 = Fuhr & Wiese (2009); E4 = Biémont et al. (2011); E5 = Biemont et al. (1981); E6 = Ljung et al. (2006); E7 = Whaling & Brault (1988); E8 = Fuhr & Wiese (2009), using hfs/IS from McWilliam (1998); E9 = Lawler et al. (2001a), using hfs from Ivans et al. (2006); E10 = Lawler et al. (2009); E11 = Li et al. (2007), using hfs from Sneden et al. (2009); E12 = Ivarsson et al. (2001), using hfs from Sneden et al. (2009); E13 = Den Hartog et al. (2003), using hfs/IS from Roederer et al. (2008) when available; E14 = Lawler et al. (2006), using hfs/IS from Roederer et al. (2008) when available; E15 = Lawler et al. (2001c), using hfs/IS from Ivans et al. (2006); E16 = Roederer et al. (2012b); E17 = Den Hartog et al. (2006); E18 = Lawler et al. (2001b), using hfs from Lawler et al. (2001d, 2009); E19 = Wickliffe et al. (2000); E20 = Lawler et al. (2008); E21 = Wickliffe & Lawler (1997); E22 = Sneden et al. (2009) for log *gf* and hfs/IS; E23 = Lawler et al. (2007); E24 = Biémont et al. (2000), using hfs/IS from Roederer et al. (2012b).

This table is published in its entirety in the electronic edition of the paper. A portion is shown here for guidance regarding its form and content.

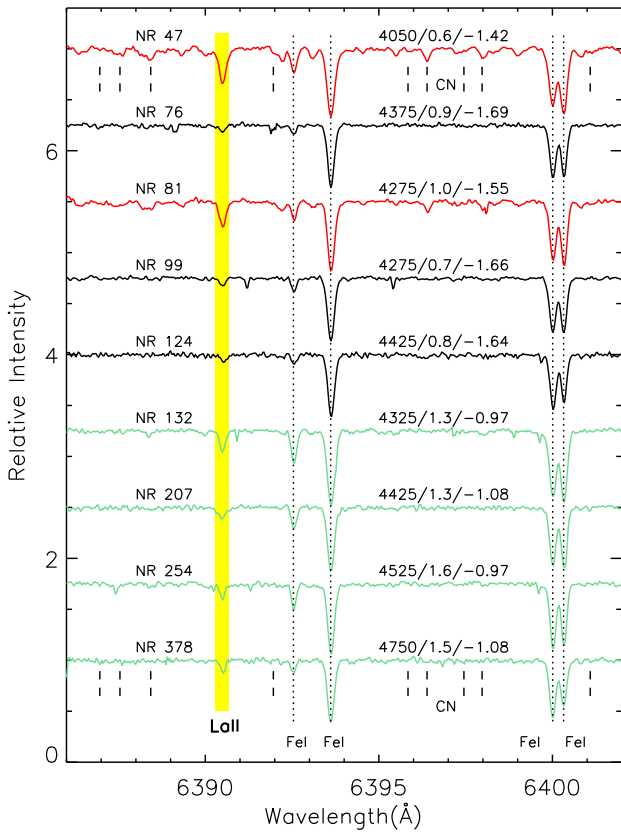


Figure 4. Same as Figure 2 but for a region containing a La line used in the analysis. There are significant star-to-star differences in the line strength of La. The positions of CN lines are marked.

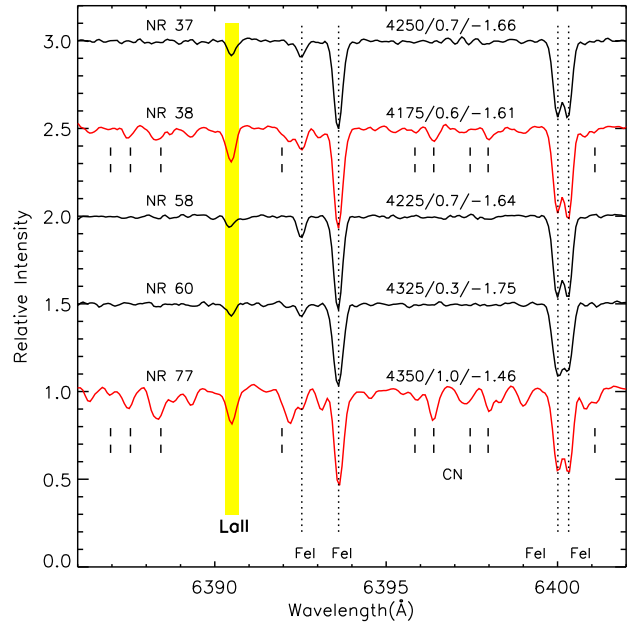


Figure 5. Same as Figure 4 but for the Magellan MIKE spectra.

(1996) catalogue⁵. The values are the weighted mean from the *b-y*, *V-J*, *V-H* and *V-K* colours (*JHK* photometry from 2MASS, Skrutskie et al. 2006). The surface gravity

⁵ Here and throughout the paper, we use the values found in the 2010 version of the catalogue (available online) rather than the values in the original Harris (1996) paper.

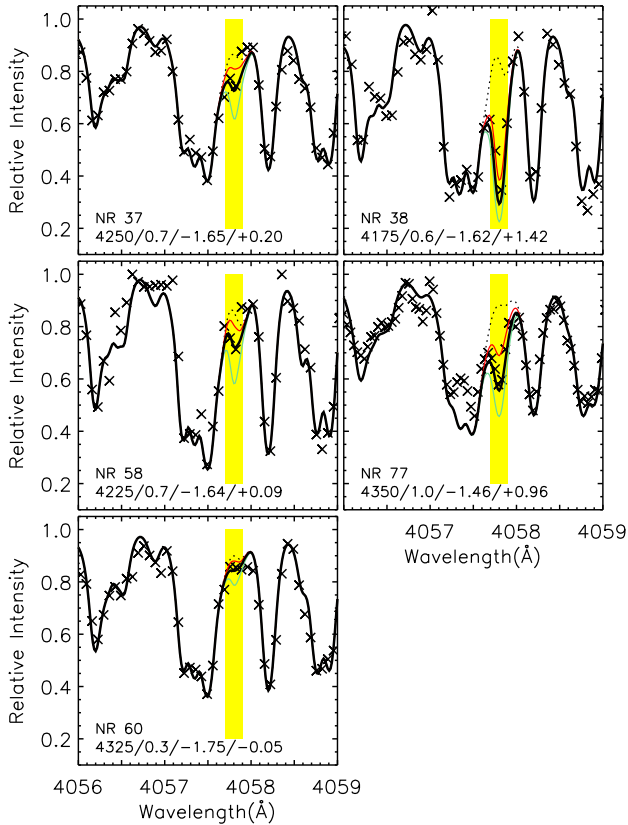


Figure 6. A portion of the Magellan MIKE spectra near the 4057 Å Pb I line, highlighted in yellow. The black thick line represents the best-fitting synthetic spectra. The red and aqua lines show synthetic spectra with unsatisfactory ratios of $[\text{Pb}/\text{Fe}]$, namely $\Delta\text{Pb} \pm 0.5$ dex from the line of best fit. The dotted black line is a synthesis containing no Pb. The values written in the bottom of each panel are $T_{\text{eff}}/\log g/[\text{Fe}/\text{H}]/[\text{Pb}/\text{Fe}]$.

was determined assuming the photometric T_{eff} , a distance modulus $(m - M)_V = 15.5$ (Harris 1996), bolometric corrections from Alonso et al. (1999) and a mass of $0.8 M_{\odot}$. The mean differences (photometric – spectroscopic) in T_{eff} and $\log g$ are -13 ± 26 K ($\sigma = 78$ K) and $+0.08 \pm 0.07$ dex ($\sigma = 0.20$ dex), respectively. These differences are within the uncertainties estimated above.

For Ni and lighter elements, chemical abundances were computed using the measured EWs, final model atmospheres and MOOG. For Cu, Zn and the neutron-capture elements, abundances were determined via spectrum synthesis (e.g., see Figure 6 for the Pb analysis). Lines affected by hyperfine splitting (hfs) and/or isotope shifts (IS) were treated appropriately using the hfs data from Kurucz & Bell (1995) or other sources as noted in Table 3. We adopted the Asplund et al. (2009) solar abundances. The chemical abundances are presented in Table 4.

To determine the errors in chemical abundances, we repeated the analysis varying the stellar parameters, one at a time, by the relevant uncertainties noted above. Additionally, we also changed the metallicity in the model, $[\text{m}/\text{H}]$, by 0.2 dex. We added these four error terms in quadrature to obtain the systematic uncertainty. We replaced the random error (s.e. $_{\log \epsilon}$) by $\max(\text{s.e.}_{\log \epsilon}, 0.20/\sqrt{N_{\text{lines}}})$ where the sec-

Table 4. Chemical abundances for the program stars.

Name	A(X)	N_{lines}	s.e. $_{\log \epsilon}$	$[\text{X}/\text{Fe}]$	Total Error
O I					
NR 37	7.48	1	...	0.44	0.23
NR 38	7.71	2	0.06	0.64	0.19
NR 47
NR 58	7.62	2	0.00	0.57	0.19
NR 60	7.20	2	0.10	0.26	0.18
NR 76
NR 77
NR 81	7.83	2	0.03	0.69	0.18
NR 99
NR 124
NR 132
NR 207
NR 254
NR 378	7.97	1	...	0.36	0.24
Na I					
NR 37	4.76	3	0.03	0.18	0.13
NR 38	4.73	3	0.06	0.11	0.13
NR 47	5.44	3	0.01	0.63	0.14
NR 58	4.44	3	0.03	-0.16	0.13
NR 60	4.84	3	0.06	0.35	0.13
NR 76	4.43	3	0.06	-0.12	0.13
NR 77	5.29	4	0.10	0.52	0.12
NR 81	4.84	5	0.02	0.15	0.11
NR 99	4.43	2	0.06	-0.14	0.15
NR 124	4.86	3	0.01	0.26	0.13
NR 132	5.14	5	0.04	-0.13	0.10
NR 207	5.01	4	0.04	-0.14	0.11
NR 254	5.08	4	0.03	-0.18	0.11
NR 378	4.93	2	0.03	-0.22	0.15
Mg I					
NR 37	6.27	4	0.03	0.33	0.11
NR 38	6.55	4	0.06	0.56	0.11
NR 47
NR 58	6.42	5	0.04	0.47	0.10
NR 60	6.27	3	0.01	0.42	0.13
NR 76	6.23	3	0.02	0.32	0.12
NR 77	6.59	4	0.05	0.46	0.11
NR 81	6.40	3	0.05	0.35	0.12
NR 99	6.38	3	0.10	0.45	0.13
NR 124	6.25	2	0.03	0.29	0.15
NR 132	6.86	4	0.04	0.22	0.11
NR 207	6.79	1	...	0.28	0.22
NR 254	6.89	1	...	0.26	0.22
NR 378	6.75	2	0.02	0.23	0.15

This table is published in its entirety in the electronic edition of the paper. A portion is shown here for guidance regarding its form and content.

ond term is what would be expected for a set of N_{lines} with a dispersion of 0.20 dex (a conservative value based on the abundance dispersion exhibited by Fe I lines). To obtain the total error (presented in Table 4), we added the systematic and random errors in quadrature.

As noted in Section 2.2, star NR 77 had a faint companion and we extracted the spectrum for this star in two different ways. In the first approach, we placed the apertures for each order in such a way as to avoid flux from the faint companion. In the second approach, we extracted the

flux from both stars. The stellar parameters and chemical abundances were essentially identical between the two approaches. We present the values from the first approach and are confident that the results for this star are not affected by contamination from the faint companion.

For the 14 stars observed at high spectral resolution, radial velocities were obtained from the observed wavelengths of the lines used in the equivalent-width analysis. Heliocentric corrections were applied and the radial velocities are presented in Table 2. For the ten stars observed at high- and medium-resolution, we find an average radial velocity difference (high-resolution – medium-resolution) of $-1.0 \pm 0.7 \text{ km s}^{-1}$ ($\sigma = 2.1 \text{ km s}^{-1}$). This agreement gives us additional confidence in our heliocentric radial velocity measurements.

4 RESULTS

4.1 Cluster membership

Cluster membership for any given star can be established through a combination of the following criteria: (i) evolutionary status, (ii) location in CMD, (iii) radial velocity, (iv) distance from cluster center and (v) proper motions. Regarding point (i), all stars selected from Strömgren CMDs have colours and magnitudes consistent with being giant stars at the distance of M2. In particular, all 14 stars observed with the Subaru Telescope or Magellan Telescope are red giants with magnitudes consistent with the distance modulus of M2. Concerning point (ii), all stars occupy plausible locations in all CMDs (although we shall revisit this aspect in Section 4.4 taking into account the derived metallicities). Regarding point (iii), the heliocentric radial velocity of M2 is $-5.3 \text{ km s}^{-1} \pm 2 \text{ km s}^{-1}$ and the central velocity dispersion is $8.2 \text{ km s}^{-1} \pm 0.6 \text{ km s}^{-1}$ (Harris 1996). While all stars have a radial velocity consistent with cluster membership, the small value means that radial velocity alone cannot confirm cluster membership. Concerning point (iv), we note that all stars lie within the tidal radius (21.45, Harris 1996). For point (v), proper motions, and membership probabilities based on those measurements, were published by Cudworth & Rauscher (1987). For the 16 stars with proper motion measurements, we note that all are high probability cluster members, $P = 99\%$.

Whether or not the four anomalous RGB stars with $[\text{Fe}/\text{H}] \approx -1.0$ are cluster members obviously affects our conclusions. We remain open to both possibilities, i.e., that these four stars may, or may not, be members. That said, in an upcoming study by Milone et al. (in preparation), recent *Hubble Space Telescope* photometry reveals that the four metal-rich stars appear to lie on a narrow well-defined RGB sequence that can be traced to the subgiant branch and main sequence regions supporting the case for cluster membership.

4.2 Radial velocity and velocity dispersion

To determine the radial velocity and velocity dispersion for M2, we took the following approach. We exclude NR 847 as this star exhibits radial velocity variation. For stars with multiple radial velocity measurements, we adopt the

weighted mean for a given star. Assuming all stars are cluster members, we find that the heliocentric radial velocity for M2 is $-3.9 \pm 1.1 \text{ km s}^{-1}$ ($\sigma = 7.0 \text{ km s}^{-1}$)⁶. These values are in good agreement with those listed in the Harris (1996) catalogue.

4.3 CN and CH indices

In the upper panel of Figure 7, we plot the $S(3839)$ index against V mag. In this figure, we include the data from Smith & Mateo (1990) and exclude the UV-bright (NR 184), HB (NR 648 and NR 707) and AGB (NR 82) stars. As discussed in Section 3.1, our measurements are on the same scale as Smith & Mateo (1990). The middle panel shows the generalised histogram of the $S(3839)$ residuals, $\delta S(3839)$, measured with respect to the same baseline as in Smith & Mateo (1990), namely $S_0(3839) = -0.1V + 1.644$. The generalised histogram was produced using a Gaussian kernel with a FWHM of 0.03. We note that while Smith & Mateo (1990) identified a particularly CN rich star (HI-240, $S(3839) = 1.110$), our sample includes an even more extreme example, NR 358 with $S(3839) = 1.394$. In the following subsection, however, we note that NR 358 (not observed at high resolution) has a CMD location inconsistent with cluster membership given the metallicity of this star assuming no significant age spread in the cluster.

In the lower panel of Figure 7, we plot the m_{CH} index against V mag. Consideration of the measurement errors would indicate a genuine spread in the m_{CH} index within this cluster. In addition to the two CH stars identified by Smith & Mateo (1990), there are three stars with $m_{\text{CH}} > 0.1$, NR 81, NR 299 and NR 1204. Given the metallicity of NR 1204, the CMD location is inconsistent with cluster membership (i.e., we use the same argument as for NR 358 above that will be described in the following subsection). We have no reason to suspect non-membership for the other two stars with strong m_{CH} indices, NR 81 and NR 299. There is no obvious anti-correlation between the $S(3839)$ and m_{CH} indices. Indeed, the two CH stars from Smith & Mateo (1990) also exhibit large $S(3839)$ indices. *The first key result is that we confirm the presence of unusually CN and/or CH strong stars in M2.*

4.4 Calcium triplet and high-resolution metallicities

Based on the iron abundances derived from the high dispersion spectra, it is clear that the anomalous RGB stars have higher $[\text{Fe}/\text{H}]$ values than those for the normal RGB stars. In particular, the six normal RGB stars in Table 2 have a mean iron abundance of $\langle [\text{Fe}/\text{H}] \rangle = -1.67 \pm 0.02$ ($\sigma = 0.04$). The eight anomalous stars separate into two metallicity groups (and in the following subsection we shall see that the two groups exhibit distinct $[\text{X}/\text{Fe}]$ ratios). The more metal-poor group of anomalous RGB stars includes four objects (NR 38, NR 47, NR 77 and NR 81) and has $\langle [\text{Fe}/\text{H}] \rangle = -1.51 \pm 0.04$ ($\sigma = 0.09$) dex. The more metal-rich group of anomalous RGB stars consists of four objects (NR 132,

⁶ This value is the observed dispersion and is not corrected for the contribution from velocity errors.

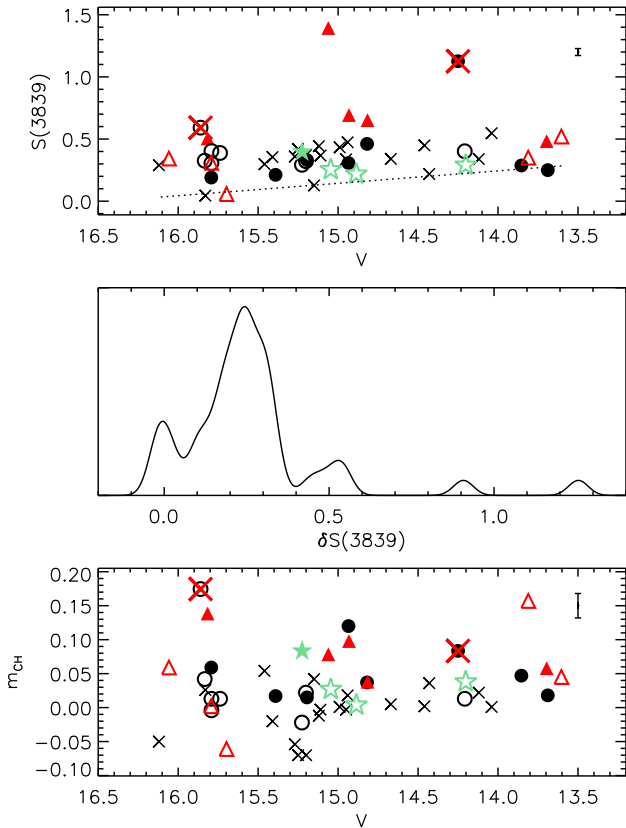


Figure 7. The $S(3839)$ CN index versus V magnitude (upper), the distribution of CN excess $\delta S(3839)$ (middle) and the m_{CH} CH index versus V magnitude (lower). (We exclude stars 82, 184, 648 and 707 since they are not on the RGB.) The program stars are shown as black circles (canonical RGB), red triangles (metal-poor anomalous RGB) and aqua stars (metal-rich anomalous RGB). Filled symbols are proper-motion members according to Cudworth & Rauscher (1987). The crosses are stars from Smith & Mateo (1990), and the two CH objects are indicated by large red crosses. A representative error bar is shown in the top and bottom panels.

NR 207, NR 254 and NR 378) and has $\langle [\text{Fe}/\text{H}] \rangle = -1.03 \pm 0.03$ ($\sigma = 0.06$) dex. When defined in this way, each of the three groups of stars (canonical RGB, metal-poor anomalous RGB and metal-rich anomalous RGB) likely have metallicities consistent with a single value, i.e., the dispersion in $[\text{Fe}/\text{H}]$ for a given group can probably be explained entirely by the measurement uncertainties. We now turn to the Ca II triplet spectra to investigate the presence of a metallicity dispersion in this cluster.

In Figure 8 we plot the sum of the EWs of the two stronger Ca II triplet lines against the magnitude difference from the horizontal branch, $V - V_{\text{HB}}$ for the M2 stars observed at this wavelength setting with AAOmega. Here the y magnitudes were assumed to be equivalent to V and the value of V_{HB} was taken from Harris (1996). “Normal” RGB stars are plotted as black circles while the triangle and star symbols show the location of stars from the anomalous RGB. The two CH-stars identified by Smith & Mateo (1990) are shown as red crosses.

In order to calibrate the line strengths in terms of $[\text{Fe}/\text{H}]$ we have made use of similar observations of red giants

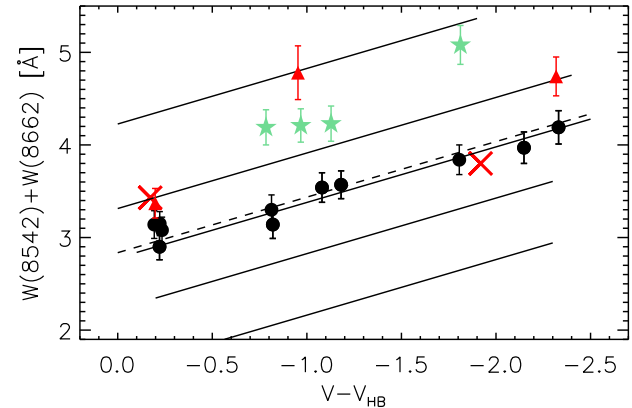


Figure 8. The sum of the EWs of the Ca II triplet lines at 8542 Å and 8662 Å are plotted against magnitude difference from the horizontal branch $V - V_{\text{HB}}$. M2 stars lying on the “normal” RGB are shown as black circles while stars from the “anomalous” RGB are plotted as red triangles or aqua star symbols. The two CH-stars identified by Smith & Mateo (1990) are shown as red crosses. The solid lines are the relations between summed EWs and $V - V_{\text{HB}}$ for the standard clusters. In order of increasing summed EW the standard clusters are NGC 7099 ($[\text{Fe}/\text{H}] = -2.27$), NGC 2298 (-1.96), NGC 1904 (-1.58), NGC 288 (-1.32) and 47 Tuc (-0.76). The dashed line is a fit of a line with slope -0.60 Å/mag to the M2 normal RGB stars.

in “standard” globular clusters that have well established abundances. The clusters are NGC 7099 (M30), NGC 2298, NGC 1904, NGC 288 and 47 Tuc. The observations for these clusters were obtained with AAOmega during the same observing run as that for the M2 Ca II triplet spectra, using an identical instrumental setup. The standard cluster stars observed were chosen using the photometry lists made publicly available by Peter Stetson at the Canadian Astronomy Data Centre⁷. A similar analysis to that described here for M2 led to the identification of RGB cluster members from the observations. The Ca II triplet line strengths of these stars were then measured using the same procedure as for the M2 stars described in Section 3.1. The numbers of confirmed RGB cluster members ranged from 8 and 10 in NGC 2298 and NGC 7099 to 33 and 46 in NGC 288 and 47 Tuc. In each cluster the RGB stars covered at least two magnitudes in $V - V_{\text{HB}}$ at luminosities exceeding $V - V_{\text{HB}} \approx 0.0$ mag, and we adopted V_{HB} from Harris (1996). A slope of -0.60 ± 0.01 Å/mag was found to fit consistently each set of cluster data. This value is similar to that found in other Ca II triplet studies: for example, Saviane et al. (2012) find a value for the slope of -0.627 while the original study of Armandroff & Da Costa (1991) found a slope of -0.619 Å/mag.

Adopting W' as the value of the summed EW at $V - V_{\text{HB}} = 0$ with the adopted slope of -0.60 Å/mag, and $[\text{Fe}/\text{H}]$ abundances from Carretta et al. (2009) for the standard clusters, then yields a very well defined linear relationship between W' and $[\text{Fe}/\text{H}]$: $[\text{Fe}/\text{H}] = 0.590 W' - 3.253$ dex. The RMS about the fitted relation is only 0.02 dex, indicating excellent consistency between the Ca II

⁷ www3.cadc-ccda.hia-ihh.nrc-cnrc.gc.ca/community/STETSON/standards/

triplet line strength measurements for these clusters and the Carretta et al. (2009) $[\text{Fe}/\text{H}]$ abundances. The relation is valid for the abundances encompassed by the standard clusters, i.e., from $[\text{Fe}/\text{H}] \approx -2.3$ to $[\text{Fe}/\text{H}] \approx -0.7$ dex.

Returning now to Figure 8, we note that the normal M2 RGB stars cluster tightly around the fitted line of slope $-0.60 \text{ \AA}/\text{mag}$, shown as the dashed line. In particular, there is no evidence for any intrinsic dispersion in $[\text{Fe}/\text{H}]$ values from the Ca II triplet line strengths of these stars. The $[\text{Fe}/\text{H}]$ abundance derived from the mean W' value is $[\text{Fe}/\text{H}]_{\text{CaT}} = -1.58 \pm 0.08$ dex, where the error includes the RMS deviation about the fitted line for the 11 normal RGB stars and the (minor) calibration uncertainty. This value of $[\text{Fe}/\text{H}]$ is somewhat higher than the value listed in Carretta et al. (2009) for M2, $[\text{Fe}/\text{H}] = -1.66 \pm 0.07$, and in the latest version of the Harris (1996) catalogue ($[\text{Fe}/\text{H}] = -1.65$). Both of these values stem from the measurement of Ca II triplet line strengths in an integrated spectrum of M2 obtained by Armandroff & Zinn (1988). The value is also somewhat higher than the mean abundance, -1.67 ± 0.02 (std. error of mean), of the six normal RGB stars observed at high dispersion.

Nevertheless, there is good agreement between the $[\text{Fe}/\text{H}]$ values derived from the Ca II line strengths and from high dispersion analysis for the three normal RGB stars in common (NR 76, 99 and 124). For these three stars, the mean difference in $[\text{Fe}/\text{H}]$, in the sense of the high dispersion values minus the Ca II values, is -0.03 ± 0.01 dex ($\sigma = 0.02$). This consistency also applies to the 5 anomalous RGB stars (NR 47, 132, 207, 254 and 378) in common between the two datasets. Here the mean difference is 0.00 ± 0.05 dex ($\sigma = 0.11$) suggesting we can combine the $[\text{Fe}/\text{H}]$ determinations for the anomalous RGB stars into a single sample. There are then 10 anomalous RGB star $[\text{Fe}/\text{H}]$ determinations, eight from the high dispersion analysis, seven from the Ca II triplet spectroscopy with five stars in common. For the latter stars the $[\text{Fe}/\text{H}]$ values have been averaged, weighted by the uncertainties. We assume for the present that all the stars are cluster members.

The mean abundance of the anomalous RGB stars is the $\langle [\text{Fe}/\text{H}] \rangle = -1.29 \pm 0.09$, considerably more metal-rich than that for the normal RGB stars, and with a substantial dispersion of 0.28 dex. The $[\text{Fe}/\text{H}]$ range shown by the anomalous RGB stars is ~ 0.8 dex indicating that there is a substantial intrinsic iron abundance spread present. Moreover, the value of the mean abundance and the size of the intrinsic abundance spread do not change significantly even if the sample is restricted to the four anomalous RGB stars with 99% membership probabilities. Further, although the sample is not large, the anomalous RGB stars appear to fall into two distinct metallicity groups, each containing 5 objects. The first, consisting of stars NR 38, 47, 77, 81 and 1204, has a mean abundance of $\langle [\text{Fe}/\text{H}]_{\text{CaT}} \rangle = -1.47 \pm 0.05$ ($\sigma = 0.11$). For the four stars in this group with high dispersion spectra, the mean abundance is $\langle [\text{Fe}/\text{H}] \rangle = -1.51 \pm 0.04$ ($\sigma = 0.09$). Similarly, for the second group of stars, NR 132, 207, 254, 358 and 378, the mean abundance is $\langle [\text{Fe}/\text{H}]_{\text{CaT}} \rangle = -0.98 \pm 0.06$ ($\sigma = 0.13$) dex and for the four stars with high dispersion spectra, the mean abundance is $\langle [\text{Fe}/\text{H}] \rangle = -1.03 \pm 0.03$ ($\sigma = 0.06$). Within each group the intrinsic abundance dispersion is notably smaller than for the full

sample, and these two groups mirror those identified by our high resolution spectroscopic analysis.

We note in passing that we have not included the two CH stars in the above discussion. Nevertheless, the Ca II triplet spectra of these two objects appear very similar to those of the other M2 stars observed. The measured line strengths imply abundances of $[\text{Fe}/\text{H}]_{\text{CaT}} = -1.69 \pm 0.11$ for HI-240 and $[\text{Fe}/\text{H}]_{\text{CaT}} = -1.29 \pm 0.12$ for HI-451. The former is consistent with that for the normal RGB stars as well that of anomalous RGB stars such as NR 38 ($[\text{Fe}/\text{H}]_{\text{CaT}} = -1.61 \pm 0.05$). The latter is similar to those for the anomalous RGB stars NR 207 ($[\text{Fe}/\text{H}]_{\text{CaT}} = -1.11 \pm 0.07$) and NR 1204 ($[\text{Fe}/\text{H}]_{\text{CaT}} = -1.34 \pm 0.09$).

In the above discussion we have implicitly assumed that the stars observed are all members of M2, deriving abundances under that assumption. There seems no reason to doubt the membership of any of the stars in the normal RGB samples. There is, however, a consistency check that we can apply to further investigate the membership status of the anomalous RGB stars. The check is as follows: given the reasonable assumption that the age range in M2 is small ($\lesssim 2$ Gyr, Piotto et al. 2012), stars that are M2 members with higher $[\text{Fe}/\text{H}]$ abundances should lie to the red of normal RGB stars at the same magnitude in the CMD by an amount that depends on the excess in $[\text{Fe}/\text{H}]$ above that for the normal RGB stars. Ideally such an investigation would use, for example, an $(I, V - I)$ CMD to minimise the potential influence of molecular bands on the photometry at bluer wavelengths. However, such photometry is not available for most of the anomalous RGB stars. We have therefore used a $(V, B - V)$ CMD based on the M2 photometry given in Stetson's Photometric Standard Star fields available from the Canadian Astronomy Data Centre. The M2 normal RGB is well-defined in this data set. We then plotted the stars observed spectroscopically in the CMD using either Stetson's photometry where available or by generating V and $(B - V)$ values from the Grundahl et al. (1999) y and $(b - y)$ photometry. Here we have $y = V$ and $(B - V) = 1.64 (b - y)$ with the latter relation determined from 11 stars in common between Stetson's photometry list and the stars observed at the Ca II triplet. The RMS deviation about the relation is only 0.009 mag.

We then use isochrones for metallicities of $[\text{Fe}/\text{H}] = -1.65, -1.25$ and -0.85 dex, $[\alpha/\text{Fe}] = +0.4$ and an age of 13 Gyr from the Dartmouth isochrone set (Dotter et al. 2008) to provide an indication of the colour shift expected for the metallicities of the anomalous RGB stars. We adopt values from the current on-line version of the Harris (1996) database for the reddening and distance modulus of M2 and with these parameters the $[\text{Fe}/\text{H}] = -1.65$ theoretical RGB is an acceptable representation of the normal RGB stars in the CMD.

Specifically, for each anomalous RGB star, we have interpolated in the isochrones at the V magnitude of the star to determine the $(B - V)$ that corresponds to the $[\text{Fe}/\text{H}]$ value. This colour, and its uncertainty derived from the uncertainty in the $[\text{Fe}/\text{H}]$ value, is then compared with the observed $(B - V)$ value. Stars NR 38, 47, 77 and 81 have predicted colours that agree well with the observed colours on the metal-poor anomalous RGB: the mean difference (observed - predicted) is 0.00 ± 0.03 with, in each case, the predicted colour lying within 2σ of the observed colour. We

conclude therefore that all four of these stars are likely to be members of the cluster: one (NR 47) has a 99% membership probability from Cudworth & Rauscher (1987) while the others are not classified. Conversely, with this approach it seems probable that stars NR 132, 358, 378 and 1204 are not members of the cluster. Here the colour differences on the metal-rich anomalous RGB are -0.18 ± 0.04 , -0.29 ± 0.04 , -0.15 ± 0.03 , and -0.08 ± 0.02 , respectively; i.e., in each case the location of the star in the CMD is at least 3.5σ bluer than predicted for the star's metallicity. The observed colours can only be reproduced if the age of the stars is at least 6 Gyr younger than the 13 Gyr assumed, which seems unlikely, although as we have already noted in passing, this argument only considers metallicity and that other elements (He, C, N, O and α elements) can also affect the $B - V$ colour. We note further that our classification contrasts with the fact that three of these stars (NR 358, 378 and 1204) have 99% membership probabilities in the Cudworth & Rauscher (1987) study.⁸ For stars NR 207 and NR 254 the comparison suggests that these stars may also be non-members: both lie in the CMD 0.10 ± 0.03 mag bluer than the predicted colour. Neither has a classification in the Cudworth & Rauscher (1987) study. For these stars we will need to rely on the similarity of their chemical abundance distributions with those of the cluster members, or with the non-members, for the membership classification.

We conclude therefore that at least some of the anomalous RGB stars, in particular the stars NR 38, NR 47, NR 77 and NR 81 (and perhaps also NR 207 and NR 254) are likely bona-fide members of M2. *If this is indeed the case then the second key result we find is that M2 joins other clusters like M22 (Da Costa et al. 2009; Marino et al. 2009, 2011), M54 (Carretta et al. 2010b; Saviane et al. 2012) and NGC 5824 (Da Costa et al. 2014) in possessing a modest intrinsic [Fe/H] range: M2 has member stars with [Fe/H] values up to 0.25 dex above that for the majority of cluster members, perhaps up to 0.7 dex depending on the membership status of the metal-rich anomalous RGB stars.*

To investigate the likelihood of observing field stars in the vicinity of M2 with stellar parameters (T_{eff} , $\log g$ and $[\text{Fe}/\text{H}]$) similar to that of the four metal-rich anomalous RGB stars observed at high resolution, we make use of the Trilegal Galactic model (Girardi et al. 2005). First, we consider all stars within a one degree square field centered on M2. Secondly, we restricted the sample to lie in the same region in the v versus $u - y$ CMD from which we selected the anomalous RGB stars. We find 17285 such stars in the Trilegal model. Thirdly, of these 17285 stars, we counted the number that satisfied the following constraints: (i) $-25 \leq \text{RV} \leq +25$ km s⁻¹ and (ii) $-1.2 \leq [\text{Fe}/\text{H}] \leq -0.8$ dex. And finally, we counted the numbers of stars that lay in a particular region in the $T_{\text{eff}}\text{-}\log g$ plane, specifically, the

area is bounded at the left edge by the line from $(T_{\text{eff}}, \log g) = (5000, 2.0)$ to $(T_{\text{eff}}, \log g) = (4300, 0.0)$, at the right edge by the line from $(T_{\text{eff}}, \log g) = (4400, 2.0)$ to $(T_{\text{eff}}, \log g) = (3700, 0.0)$ both with $0.0 \leq \log g \leq 2.0$. We found 46 stars in the Trilegal model that satisfied all criteria and therefore estimate that given a sample of stars occupying similar locations in the v versus $u - y$ CMD as the program stars, the probability of observing a field star with stellar parameters and a radial velocity consistent with the metal-rich population is roughly 0.3%. We reach similar conclusions when using the Besançon model (Robin et al. 2003). Accurate proper-motion and parallax measurements from GAIA will establish cluster membership, or otherwise, for the M2 stars.

Given the strong bias towards anomalous RGB stars in the samples selected for observation here, we have little constraint on the form of the iron abundance distribution function other than noting that the normal RGB population is dominant and the anomalous RGB is not prominent (e.g., Lardo et al. 2012). In this context, the anomalous fainter subgiant branch contains only a small fraction of stars, $\sim 4\%$, relative to the dominant brighter subgiant branch (Piotto et al. 2012). An unbiased sample of RGB stars is needed to constrain the iron abundance distribution and allow comparison with those of other clusters. We now examine the element-to-iron abundance ratios from the high dispersion spectra of the normal and anomalous RGB stars.

4.5 Chemical Abundance Ratios

In Figure 9, we plot combinations of the light elements (O, Na, Mg, Al and Si) against one another. M2 exhibits star-to-star abundance variations of the light elements along with the usual correlations and anti-correlations between these elements found in globular clusters (e.g., see reviews by Smith 1987; Kraft 1994; Gratton et al. 2004, 2012). In particular, we note that the observed dispersions in $[\text{X}/\text{Fe}]$ for Na, Al and Si are considerably larger than the average measurement uncertainties indicating genuine abundance spreads. The six canonical RGB stars (black circles in Figure 9) clearly exhibit abundance dispersions for Na and Al as well as a correlation between these elements. The four metal-poor anomalous RGB stars (red triangles in Figure 9) also exhibit these abundance patterns and this would suggest that they are cluster members. The four metal-rich anomalous RGB stars (aqua star symbols in Figure 9) do not exhibit abundance variations for Na and Al. On the other hand, Si does not usually exhibit a star-to-star abundance variation within a given cluster, with a handful of exceptions including NGC 6752 (Yong et al. 2005) and NGC 4833 (Carretta et al. 2014). For O and Mg, there is no compelling evidence for an abundance dispersion within our sample.

Next, in Figure 10, we plot $[\text{X}/\text{Fe}]$ versus $[\text{Na}/\text{Fe}]$ for six neutron-capture species (Y, Zr, La, Nd, Eu and Pb). While there is no evidence for any significant trend between $[\text{X}/\text{Fe}]$ versus $[\text{Na}/\text{Fe}]$, it is clear that the four stars on the anomalous RGB with $[\text{Fe}/\text{H}] \approx -1.5$ exhibit large overabundances of the s -process elements with respect to the six stars on the canonical RGB. Such a result is not unexpected given the clear star-to-star line strength differences for neutron-capture elements seen in Figures 2 to 5. Confirmation of the presence of a large spread in

⁸ As discussed in Cudworth & Rauscher (1987), the proper motions membership probabilities are based on a relative system with the zero point set by the mean of all the measurements. Since the M2 sample is dominated by cluster members (see Table II of Cudworth & Rauscher 1987) whose absolute proper motions will be small given the large distance, any relatively distant field star, as distinct from nearby dwarfs, will likely also have a small proper motion and therefore potentially be assigned an erroneous high membership probability.

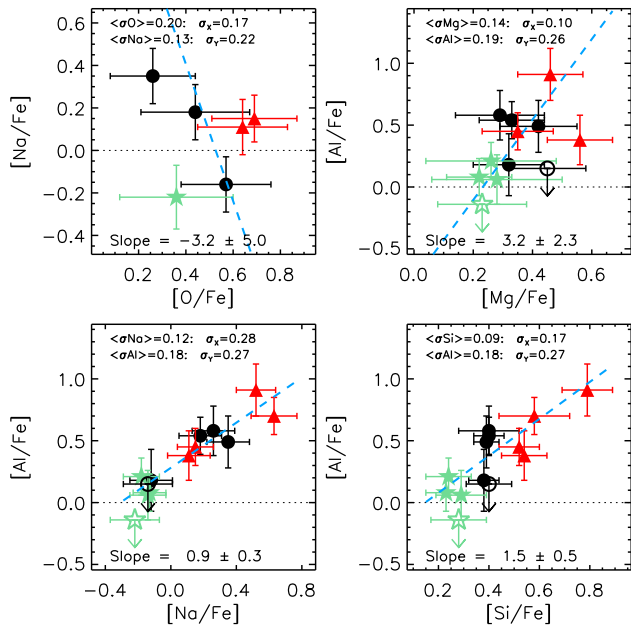


Figure 9. Abundance ratios for combinations of the light elements (O, Na, Mg, Al and Si) for the stars observed at high spectral resolution. The black points are stars on the canonical RGB while the red and aqua points are stars on the anomalous RGB. The aqua points are the unusually metal-rich objects. Open symbols reflect upper limits. The dashed blue line is the linear fit to the data (slope and error are included). The average error ($\langle \sigma[X/Fe] \rangle$) and dispersion (σ) in the x-direction and y-direction are included.

neutron-capture element abundances can be obtained by noting that the observed dispersion exceeds the average measurement uncertainty. *The third key result is that we identify an intrinsic abundance dispersion for the neutron-capture elements in M2 thereby verifying and extending the results of Lardo et al. (2013).* M2 joins the small, but growing, group of globular clusters that exhibit abundance variations for the neutron-capture elements as well as iron abundance dispersions. These clusters include ω Cen, M22 and NGC 1851 (Norris & Da Costa 1995a; Smith et al. 2000; Yong & Grundahl 2008; Marino et al. 2009, 2011; Villanova et al. 2009; Johnson & Pilachowski 2010; Carretta et al. 2011; D’Orazi et al. 2011; Roederer et al. 2011). Additionally, there are other globular clusters with a dispersion in neutron-capture element abundances, but no obvious iron abundance dispersion including M15 (Snedden et al. 1997, 2000; Otsuki et al. 2006; Sobeck et al. 2011; Worley et al. 2013) and NGC 362 (Carretta et al. 2013).

In Figure 11 we plot $[X/Fe]$ versus $[Fe/H]$ for the program stars and field stars from Fulbright (2000). Here one sees that the six M2 giants on the canonical RGB appear to follow the trends exhibited by field halo stars (although we recognise that there may be systematic abundance differences between this analysis and that of Fulbright 2000). Similarly, in this figure the four *s*-process rich stars with $[Fe/H] \approx -1.5$ have $[X/Fe]$ ratios (excluding Y and Zr) consistent with field stars at the same metallicity. For both sets of stars, Na and Al may exhibit higher abundance ratios compared to field stars at the same metallicity. For the four

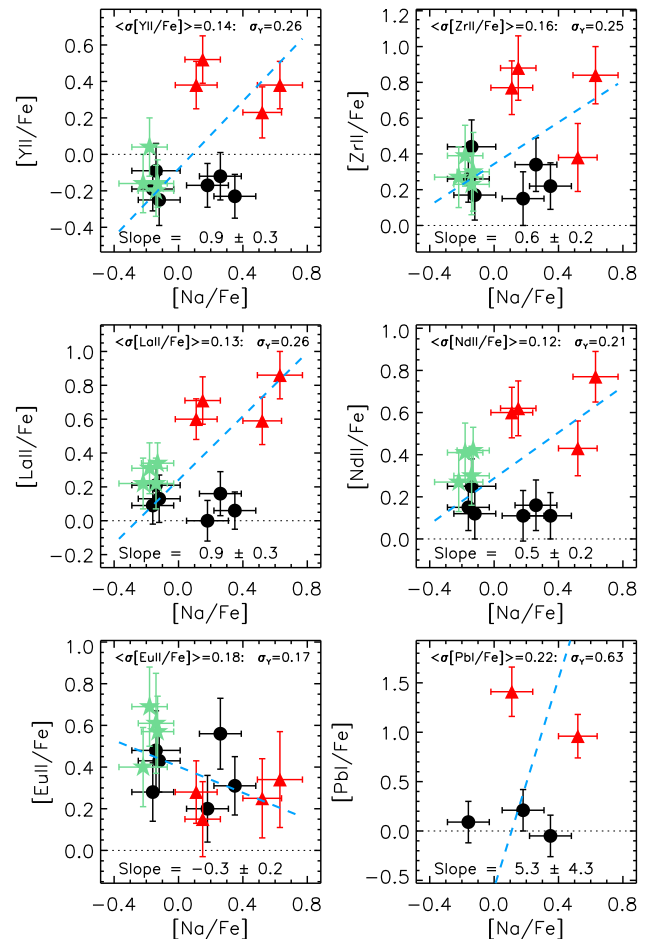


Figure 10. Same as Figure 9 but for neutron-capture elements versus $[Na/Fe]$.

metal-rich stars with $[Fe/H] \approx -1.0$, the abundance ratios for all elements included in this figure are consistent with field stars of comparable metallicity.

In Figure 12, we compare the average measurement errors⁹ with the observed dispersion in $[X/Fe]$ ratios for the three groups of stars: (1) the six canonical RGB objects (NR 37, 58, 60, 76, 99 and 124), (2) the four *s*-process rich anomalous RGB stars (NR 38, 47, 77 and 81) and (3) the four metal-rich anomalous RGB stars (NR 132, 207, 254, 378). For the second group, all are likely members based on our analysis in the previous subsection whereas for the third group, their membership is questionable based on the analysis presented in Section 4.4, although *Hubble Space Telescope* photometry suggests that these stars may indeed be members (Milone et al. in preparation). For reasons that will become clearer in the following section, we refer to the three groups as the *r*-process only group (“*r*-only”), the *r*- + *s*-process group (“*r* + *s*”) and the “metal-rich” groups, respectively. For the purposes of this exercise, we assumed that the $[Al/Fe]$ limits are detections, and therefore the observed dispersion for $[Al/Fe]$ in the *r*-only group is effectively a lower limit. In general, there is a suggestion

⁹ For a given element in a set of stars, the “average measurement error” is the average of the Total Error presented in Table 4.

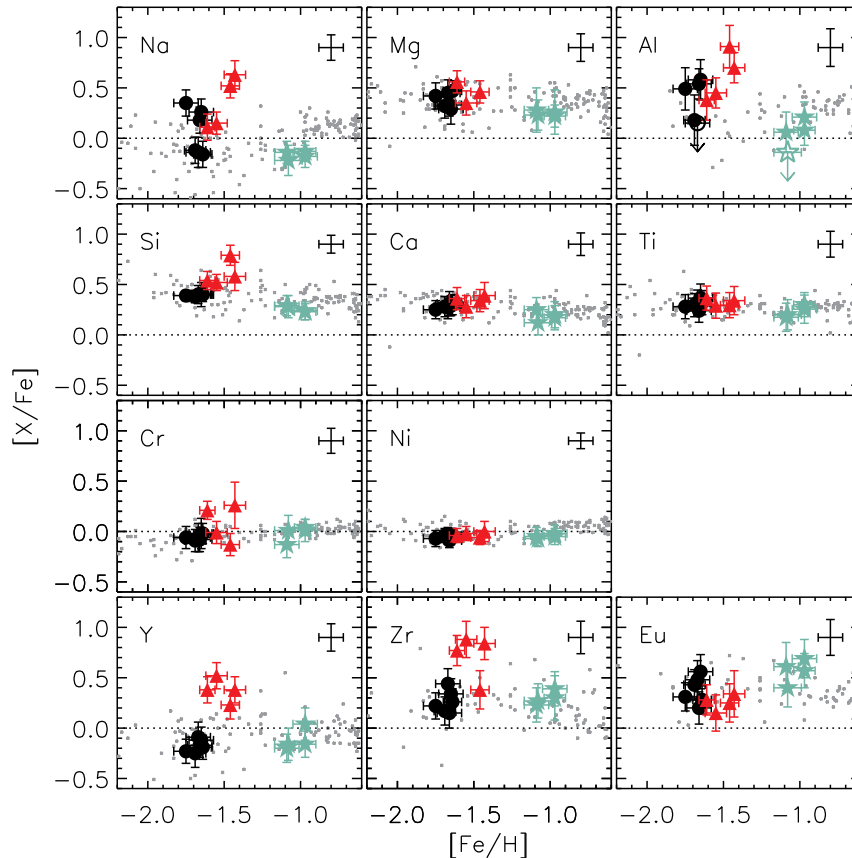


Figure 11. Abundance ratios $[X/Fe]$ versus $[Fe/H]$ for the program stars observed at high spectral resolution. The colours are the same as in Figure 9. The grey symbols are field halo stars taken from Fulbright (2000).

that the abundance errors are overestimated as the majority of elements lie below the 1:1 relation. For the r -only group, only Na (and perhaps Al) exhibits an abundance dispersion that significantly exceeds the average measurement error. For the $r + s$ group, a handful of elements including Na, Al, Cr, Zn, Zr and Ba exhibit abundance dispersions that exceed the average measurement error. For the metal-rich group, all elements exhibit abundance dispersions that are consistent with the expected dispersion given the average measurement error. That said, it is important to emphasise that for most elements, there is no evidence for an intrinsic abundance dispersion within a given group of stars. That is, with the exception of a few elements in the “ r -only” and “ $r + s$ ” groups, the dispersion in $[X/Fe]$ is consistent with the measurement error.

5 DISCUSSION

The aim of this discussion is to examine the nature of M2 in light of the chemical abundance ratios with an emphasis on the neutron-capture elements (Sections 5.2 and 5.3). In Table 5, we present the average abundance ratios and dispersions for $\log \epsilon(X)$ and $[X/Fe]$ for the r -only, $r + s$ and metal-rich groups of stars.

M2 shares similar, and peculiar, characteristics found in the unusual globular clusters M22, NGC 1851 and ω Cen, namely, a dispersion in metallicity and neutron-capture

abundance ratios. If a subset of the metal-rich group are genuine cluster members, then M2 would host stars that span a range in metallicity from $[Fe/H] \approx -1.6$ to $[Fe/H] \approx -1.0$, a factor of four. We note further that even if the most metal-rich stars are not members, there still remains a metallicity spread of order 0.25 dex among the stars for which we assert cluster membership.

M2 appears to be different from M22 and NGC 1851; for the latter two clusters, the number of stars on the bright subgiant branch is similar to the number on the faint subgiant branch. In contrast, for M2 the canonical RGB stars represent the overwhelming majority of stars. As noted in Section 4.4, the relative numbers of canonical and anomalous RGB stars in M2 is probably comparable to the relative numbers of bright ($\sim 96\%$) and faint ($\sim 4\%$) subgiant branch stars (Piotto et al. 2012).

5.1 Light-, α - and Fe-peak elements

Regarding the light elements, even with our limited sample it is apparent that the r -only and $r + s$ groups both exhibit star-to-star abundance variations and correlations between $[Na/Fe]$ and $[Al/Fe]$. The two populations in M22 and NGC 1851 both exhibit a O-Na anticorrelation (Marino et al. 2011; Carretta et al. 2011), and for ω Cen, the O-Na anticorrelation is present across a broad metallicity range (Norris & Da Costa 1995b; Johnson & Pilachowski 2010).

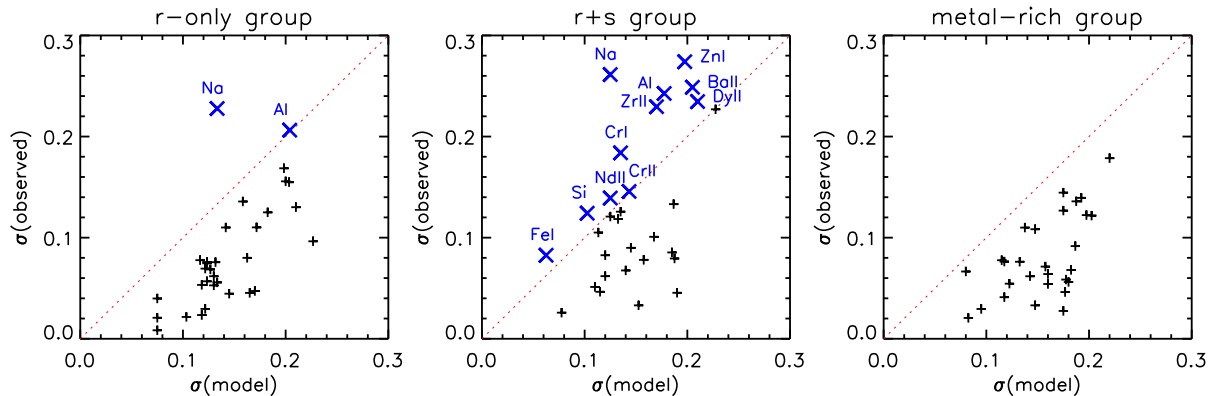


Figure 12. Measured abundance dispersion $\sigma(\text{observed})$ versus average measurement error $\sigma(\text{model})$ for the r -only (left panel), $r + s$ (middle panel) and metal-rich (right panel) groups. The dotted red line is the 1:1 relation. Elements which fall on or above the 1:1 relation are plotted as large blue crosses and the species names are written.

Indeed, every well studied Galactic globular cluster exhibits star-to-star abundance variations for the light elements C, N, O, F, Na, Mg and Al (e.g., see reviews by Kraft 1994; Gratton et al. 2004; Gratton et al. 2012). While these abundance variations are believed to be produced through hydrogen-burning, the specific site continues to be debated (e.g., Fenner et al. 2004; Ventura & D’Antona 2005; Decressin et al. 2007; de Mink et al. 2009).

For the metal-rich group, the apparent absence of a star-to-star abundance variation for the light elements is intriguing, although the sample size is small. No such abundance spread would be expected if these were all field stars. On the other hand, a similar situation is present in the M54+Sagittarius (Sgr) system. While the O-Na anticorrelation is evident in M54, the more metal-rich Sgr stars do not exhibit this pattern (Carretta et al. 2010a). If the four stars in the metal-rich group are indeed cluster members, then M2 would share this peculiar feature with M54+Sgr.

For the α and Fe-peak elements, there is no compelling evidence for a star-to-star abundance variation within a given group. Additionally, the abundance ratios $[X/\text{Fe}]$ for a given star are compatible with field stars at the same metallicity. In other words, these elements appear to be well-behaved.

The abundance of Cu offers an important tool to distinguish between field stars and “ ω Cen-like” systems. For M2, the Cu abundance may help establish additional similarities with ω Cen and potentially cluster membership, or otherwise, for the four metal-rich objects for the following reasons. In the metallicity regime $-2.0 \lesssim [\text{Fe}/\text{H}] \lesssim -0.5$, field stars exhibit a systematic increase in $[\text{Cu}/\text{Fe}]$ with increasing metallicity (e.g., Sneden & Crocker 1988; Mishenina et al. 2002; Primas & Sobeck 2008). Mono-metallic globular clusters in the same metallicity range appear to follow the field star trend (Simmerer et al. 2003). ω Cen, however, displays a near constant Cu abundance, $[\text{Cu}/\text{Fe}] \approx -0.5$, over the range $-1.9 \leq [\text{Fe}/\text{H}] \leq -0.8$ (Cunha et al. 2002). At higher metallicities, $-1.2 \leq [\text{Fe}/\text{H}] \leq -0.4$, there is evidence for an increase in the $[\text{Cu}/\text{Fe}]$ ratio in ω Cen (Pancino et al. 2002), although the rate of that increase is smaller than in field stars. Chemical evolution models of ω Cen and the Milky Way by Romano & Matteucci (2007) attribute the nucle-

osynthesis of Cu to massive stars and successfully reproduce the observed trends.

In Figure 13, we plot $[\text{Cu}/\text{Fe}]$ versus $[\text{Fe}/\text{H}]$ for M2, field stars (Mishenina et al. 2002), mono-metallic globular clusters (Simmerer et al. 2003) and ω Cen (Cunha et al. 2002; Pancino et al. 2002). The Cu abundances in M2 displayed in this figure have been adjusted in the following manner. Following Simmerer et al. (2003), the abundances from the 5105 Å and 5782 Å lines are referenced to solar values of $\log \epsilon_{\odot} = 4.21$ and $\log \epsilon_{\odot} = 4.06$, respectively. Such an approach reflects the different solar abundances obtained from these lines, and we note that the abundances we derive for program stars from the 5782 Å line are, on average, 0.21 dex \pm 0.03 dex ($\sigma = 0.11$ dex) higher than those from the 5105 Å line. The gradient of the linear fit to M2 is not affected by these zero-point offsets. We also stress that although this figure includes data from numerous studies, the linear fit in each panel is performed upon data obtained from a single study (for the lower left panel, M2, M22 and NGC 1851 are from different studies but those data are not included in the linear fit). So long as each sample is analysed uniformly, the slopes should be robust and we can compare them in a quantitative manner. In Figure 13, the slopes for the field stars and mono-metallic globular clusters are in good agreement, and these slopes differ from that seen in ω Cen. The behaviour of the slope of $[\text{Cu}/\text{Fe}]$ versus $[\text{Fe}/\text{H}]$ in M2—whether or not the $r + s$ stars are considered—is different from the field stars, mono-metallic globular clusters and ω Cen over the metallicity range $-1.7 \leq [\text{Fe}/\text{H}] \leq -0.9$. The metal-rich stars, relative to the r -only and $r + s$ groups, do not follow the field star trend, and this may be the strongest abundance-based evidence that they are cluster members. Furthermore, if the metal-rich stars are indeed cluster members, then M2 does not share a similar chemical enrichment history to ω Cen, at least for Cu. Figure 13 also demonstrates that the mean $[\text{Cu}/\text{Fe}]$ ratios in NGC 1851 (Carretta et al. 2011) and the r -only groups in M2 and M22 (Roederer et al. 2011) match the trends established by the mono-metallic globular clusters. The Cu in the $r + s$ group of stars may include small contributions from s -process nucleosynthesis, so we do not discuss Cu in the $r + s$ group here.

Table 5. Mean chemical abundances for the three groups of stars.

Species	<log ϵ > σ^a <[X/Fe]> σ				<log ϵ > σ <[X/Fe]> σ				<log ϵ > σ <[X/Fe]> σ			
	Six stars in the r -only group				Four stars in the $r + s$ group				Four stars in the “metal-rich” group			
O I	7.43	0.21	0.42	0.16	7.77	0.08	0.66	0.04	7.97	...	0.36	...
Na I	4.63	0.21	0.06	0.23	5.07	0.34	0.35	0.26	5.04	0.09	-0.17	0.04
Mg I	6.30	0.08	0.38	0.08	6.51	0.10	0.46	0.11	6.82	0.06	0.25	0.03
Al I	5.22	0.20	0.45	0.18	5.55	0.32	0.61	0.24	5.56	0.13	0.12	0.08
Si I	6.23	0.05	0.40	0.01	6.61	0.19	0.61	0.12	6.74	0.03	0.26	0.03
Ca I	4.95	0.06	0.28	0.02	5.17	0.11	0.34	0.05	5.50	0.09	0.19	0.05
Sc II	1.45	0.09	-0.03	0.06	1.58	0.10	-0.06	0.08	1.99	0.12	-0.13	0.06
Ti I	3.45	0.05	0.17	0.02	3.75	0.13	0.32	0.05	4.07	0.14	0.14	0.08
Ti II	3.70	0.09	0.43	0.07	3.76	0.06	0.33	0.09	4.24	0.11	0.32	0.05
Cr I	3.91	0.06	-0.06	0.03	4.21	0.19	0.08	0.18	4.60	0.13	-0.02	0.08
Cr II	4.11	0.10	0.14	0.08	4.22	0.07	0.12	0.15	4.74	0.15	0.11	0.09
Mn I	3.34	0.07	-0.41	0.05	3.51	0.03	-0.41	0.06	4.04	0.12	-0.36	0.07
Fe I ^b	5.82	0.04	-1.68	0.04	5.99	0.08	-1.51	0.08	6.47	0.07	-1.03	0.07
Fe II ^b	5.83	0.06	-1.66	0.06	5.99	0.10	-1.51	0.10	6.48	0.06	-1.02	0.06
Co I	3.19	0.02	-0.13	0.05	3.46	0.10	-0.02	0.07	3.87	0.11	-0.11	0.05
Ni I	4.49	0.05	-0.05	0.02	4.68	0.10	-0.03	0.03	5.14	0.08	-0.05	0.02
Cu I	1.84	0.07	-0.68	0.05	2.28	0.13	-0.40	0.09	2.63	0.19	-0.53	0.13
Zn I	2.93	0.13	0.04	0.11	3.13	0.29	0.08	0.27	3.56	0.10	0.02	0.14
Sr I	0.63	0.07	-0.56	0.10	1.31	0.20	-0.04	0.23	1.22	0.22	-0.62	0.18
Y II	0.36	0.09	-0.18	0.06	1.07	0.11	0.38	0.12	1.06	0.16	-0.12	0.11
Zr I	0.83	0.15	-0.08	0.17	1.62	0.07	0.56	0.05	1.56	0.12	0.01	0.06
Zr II	1.17	0.13	0.26	0.11	1.78	0.22	0.72	0.23	1.85	0.13	0.30	0.07
Mo I	0.10	...	-0.03
Ba II	0.69	0.17	0.19	0.15	1.59	0.28	0.92	0.25	1.45	0.16	0.30	0.12
La II	-0.47	0.09	0.11	0.07	0.28	0.18	0.69	0.13	0.34	0.13	0.27	0.06
Ce II	-0.10	0.09	-0.01	0.07	0.57	0.14	0.50	0.12	0.72	0.09	0.16	0.03
Pr II	-0.88	0.07	0.08	0.04	-0.30	0.08	0.49	0.03	-0.12	0.20	0.19	0.14
Nd II	-0.10	0.08	0.15	0.05	0.51	0.17	0.61	0.14	0.74	0.14	0.35	0.08
Sm II	-0.45	0.10	0.26	0.08	-0.12	0.10	0.43	0.08	0.44	0.17	0.50	0.11
Eu II	-0.78	0.15	0.38	0.14	-0.74	0.14	0.25	0.08	0.06	0.17	0.57	0.12
Gd II	-0.28	0.09	0.33	0.08	-0.05	0.06	0.43	0.13	0.80	...	0.70	...
Tb II	-1.13	0.07	0.27	0.14
Dy II	-0.25	0.14	0.33	0.12	0.12	0.16	0.56	0.23
Er II	-0.68	...	0.05
Tm II	-1.84	...	-0.19
Yb II	-0.94	0.14	-0.08	0.07
Hf II	-0.77	0.06	0.08	0.13	-0.27	0.11	0.42	0.00
Pb I	0.15	0.18	0.08	0.13	1.40	0.21	1.18	0.32

^a These values are the standard deviation.

^b This is [Fe I/H] or [Fe II/H], not <[X/Fe]>.

5.2 Neutron-capture abundance patterns in M2

We now turn our attention to the neutron-capture elements. In the abundance analysis described in Section 3.2, we examined up to 122 lines of elements with atomic numbers $Z \geq 38$ in each of the program stars. All abundances were computed by matching synthetic spectra, generated using one dimensional plane-parallel model atmospheres, to the observed spectra under the assumption that LTE holds in the line-forming layers.

The abundances of Sr and Pb were derived from neutral lines. For the program stars, Sr I and Pb I are minority species, and LTE calculations will tend to underestimate the populations of the lower levels of the Sr I 4607 Å and Pb I 4057 Å transitions. Abundances of strontium and lead derived in LTE from these lines are thus underestimated. Calculations allowing for departures from LTE in the line-

forming layers by making reasonable assumptions for the photoionization cross sections have been made for stars with stellar parameters similar to those in our sample. These non-LTE calculations suggest that our LTE analysis may underestimate the strontium abundance by ≈ 0.3 – 0.5 dex (Bergemann et al. 2012; Hansen et al. 2013) and the lead abundance by ≈ 0.3 – 0.4 dex (Mashonkina et al. 2012). The values presented in our tables and figures reflect the LTE values. Neglecting the non-LTE corrections for these two elements should not significantly affect any of the abundance differences between the r -only and $r + s$ groups of stars that we shall discuss below.

Figure 14 illustrates the heavy element abundance patterns found in each star of our sample. The six stars shown in the left-hand panels are those on the canonical RGB, the four stars in the middle panels are the neutron-capture rich anomalous RGB stars and the four stars in the right-hand

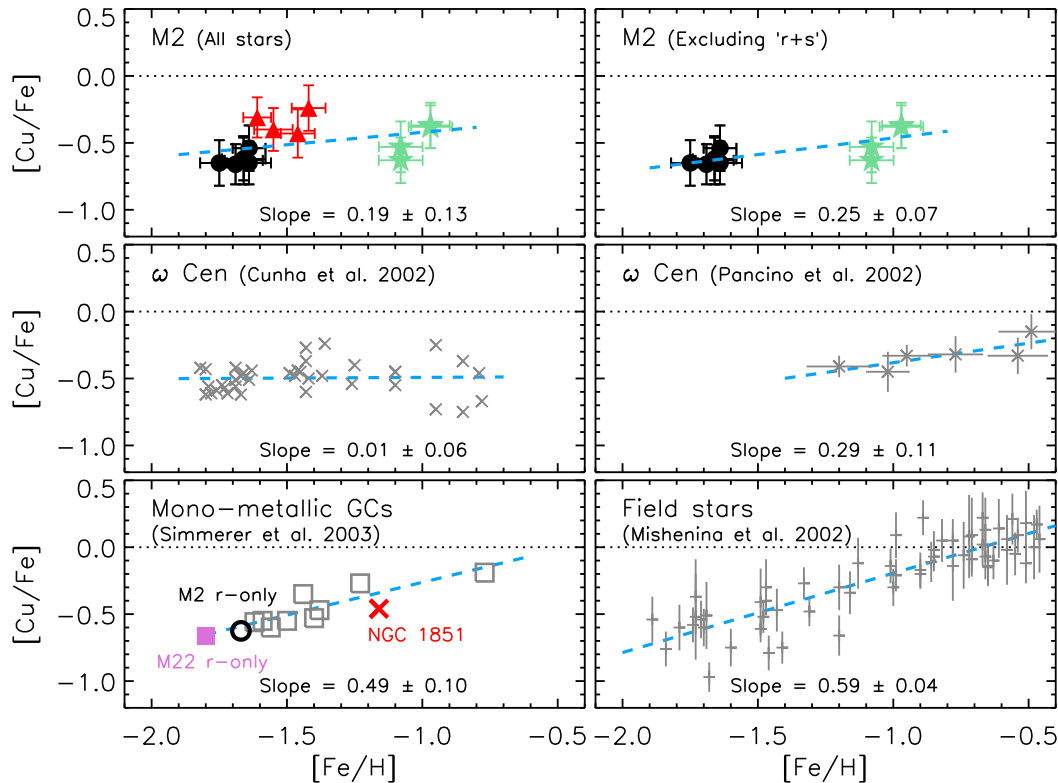


Figure 13. $[\text{Cu}/\text{Fe}]$ versus $[\text{Fe}/\text{H}]$ for M2, ω Cen (Cunha et al. 2002; Pancino et al. 2002), mono-metallic globular clusters (Simmerer et al. 2003) and field stars (Mishenina et al. 2002). In each panel, we plot the linear fit to the data and write the slope and uncertainty of the fit. For M2, our values are adjusted onto the Simmerer et al. (2003) scale (see text for details). In the lower left panel, we also include values for the M2 r -only (metal-poor) group, M22 r -only group (Roederer et al. 2011) and NGC 1851 (Carretta et al. 2011), although these values are not included in the linear fit to the data.

panels are the metal-rich anomalous RGB stars. For comparison, in each panel of this figure we overplot the heavy element abundance pattern found in the r -process rich standard star BD+17° 3248 (normalised to the Eu abundance), whose metallicity is only a factor of ≈ 2.5 lower than the majority of stars in M2. The stars on the canonical RGB have heavy element abundance patterns very similar to one another and to the r -process pattern in BD+17° 3248, and the overall amounts of heavy elements are constant within their mutual uncertainties. We refer to these six stars (NR 37, NR 58, NR 60, NR 76, NR 99 and NR 124) on the canonical RGB as the “ r -only group.” The reasoning behind this name will be made clear shortly.

As shown in the middle panels of Figure 14, the heavy elements in the neutron-capture rich anomalous RGB stars in M2 tell a different story. All heavy elements except europium in these four stars exhibit noticeable abundance enhancements relative to the stars on the canonical RGB and, therefore, enhancements relative to the r -process standard BD+17° 3248. The pattern changes little from one star to the next, and the overall abundances in this group of stars are also constant within their mutual uncertainties. We refer to these four stars (NR 38, NR 47, NR 77 and NR 81) as the “ $r + s$ group.”

The consistent patterns and levels of enhancement found within each of the r -only and $r + s$ groups suggests that we can average together their abundances to reduce the ran-

dom uncertainties, which is especially helpful for elements whose abundances are derived from small numbers of lines. These mean abundance patterns are listed in Table 5 and illustrated in Figure 15. Subtle differences between the stars in the r -only group and BD+17° 3248, (e.g., small overabundances in M2 for strontium, yttrium, zirconium, barium, cerium and neodymium, as well as small underabundances in M2 for ytterbium) may simply reflect differing combinations of material produced by the so-called weak and main components of the r -process enriching M2 and BD+17° 3248. This is plausible because the overall level of r -process enhancement relative to iron is different in BD+17° 3248 and M2, with $[\text{Eu}/\text{Fe}] = +0.9$ and $+0.4$, respectively. Regardless, Figure 14 demonstrates that the heavy elements in the stars in the r -only group in M2 owe their origin to r -process nucleosynthesis with little or no s -process contributions.

In contrast, the middle panels of Figure 14 demonstrate that the $r + s$ stars have abundance patterns that are inconsistent with r -process nucleosynthesis alone. Figure 16 demonstrates that the excess of heavy elements ($Z \geq 38$) found in the $r + s$ group relative to the r -only group exhibits an unmistakable correlation with the fraction of each element attributed to an s -process origin in solar system material. Elements with a high s -process fraction in the solar system are most overabundant in the $r + s$ group in M2, and those with small s -process fractions in the solar system show little excess. Only a few percent of the europium in

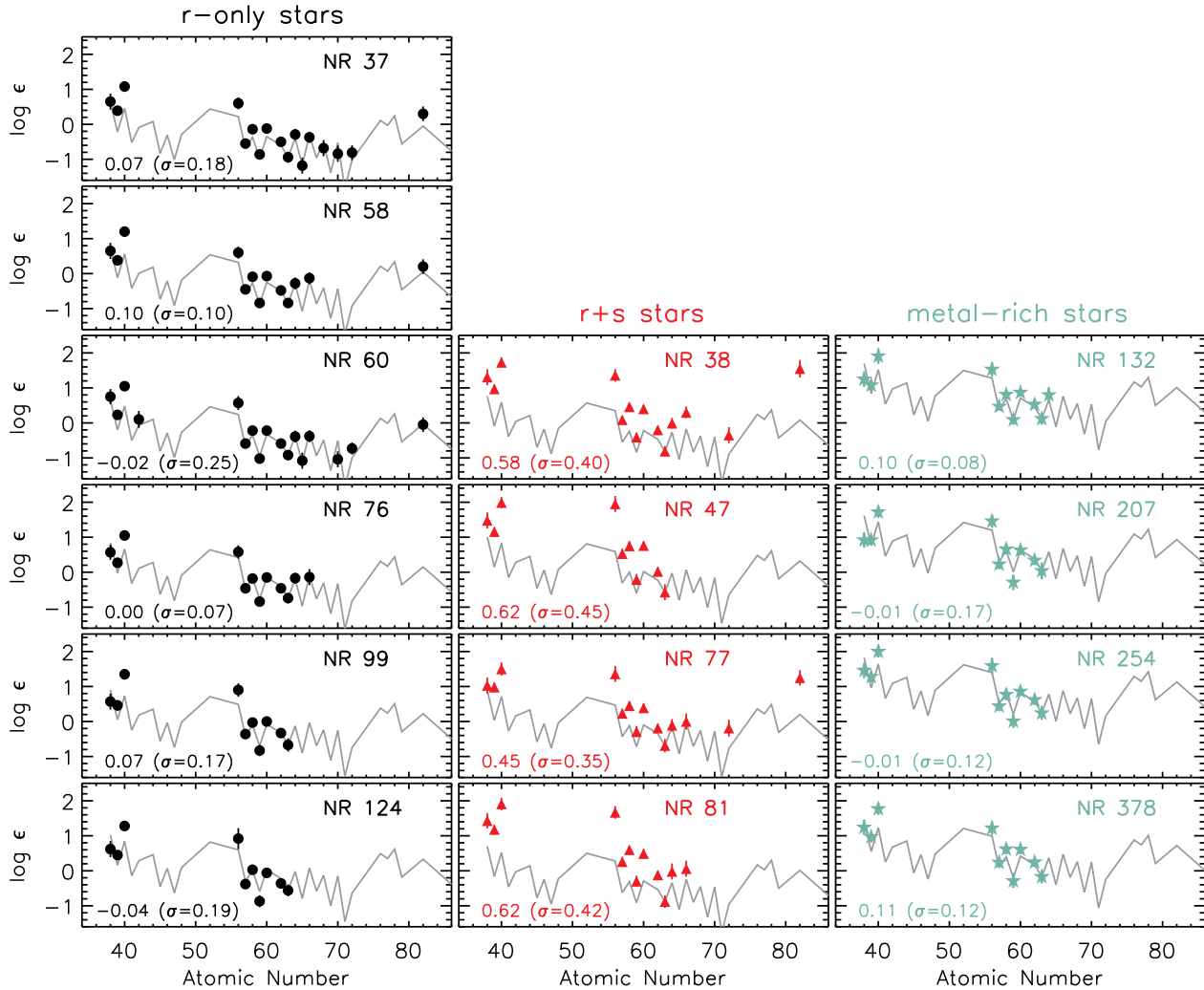


Figure 14. Logarithmic abundances for $Z \geq 38$ elements in the six r -only stars (black circles, left panels), the four $r + s$ stars (red triangles, middle panels) and the four metal-rich stars (aqua stars, right panels). For zirconium, the abundance plotted is the value derived from Zr II lines. The grey line illustrates the abundances in the r -process standard star BD+17° 3248 (Cowan et al. 2002, 2005; Sneden et al. 2009; Roederer et al. 2010b, 2012a) normalised to the europium abundance in each star. Lead has not been detected in BD+17° 3248, so we instead show the predicted Pb/Eu ratio based on the average Pb/Eu observed in Figure 3 of Roederer et al. (2010a). The numbers in the lower left corner of each panel are the mean difference “star – BD+17° 3248” and the dispersion (standard deviation) for the elements from Ba to Hf.

the solar system is attributed to s -process nucleosynthesis, and this element shows a constant abundance in both the r -only and $r + s$ groups of stars; the average $\log \epsilon$ (Eu) and [Eu/Fe] ratios are very similar between these two groups. This suggests that there is a common r -process abundance foundation in each star in the r -only and $r + s$ groups in M2. (We set aside, for now, the metal-rich group.) Following Roederer et al. (2011), we speculate that the stars in the $r + s$ group formed from additional material enriched by products of s -process nucleosynthesis as well as iron. We emphasise that the abundance differences between these two groups of stars should be nearly insensitive to any non-LTE effects given the modest range in stellar parameters (T_{eff} , $\log g$, [Fe/H]) spanned by the sample.

We now consider the metal-rich group (stars NR 132, NR 207, NR 254 and NR 378) shown in the right-hand panels of Figure 14 noting that these stars may, or may not,

be cluster members. The heavy element abundances in the metal-rich group closely resemble an r -process pattern, despite the fact that the overall metallicity of these objects is a factor of ≈ 4 higher than the other cluster members. Furthermore, the [X/Fe] ratios (where X denotes any element with $Z \geq 56$) in the metal-rich group are on average $0.17 \text{ dex} \pm 0.02 \text{ dex}$ ($\sigma = 0.05 \text{ dex}$) higher than in the r -only stars, i.e., a factor of ≈ 1.5 . If we assume that the overall metal content in an isolated stellar system increases monotonically with time, the metal-rich group should have formed later than either the r -only or $r + s$ groups. To the best of our knowledge, no isolated self-enriched stellar system shows a return to r -process dominance after previous enrichment by a substantial amount of s -process material. We conclude that the four metal-rich stars cannot be easily understood as members of a single self-enriched stellar system. That said, the data do not preclude a scenario in which M2 is com-

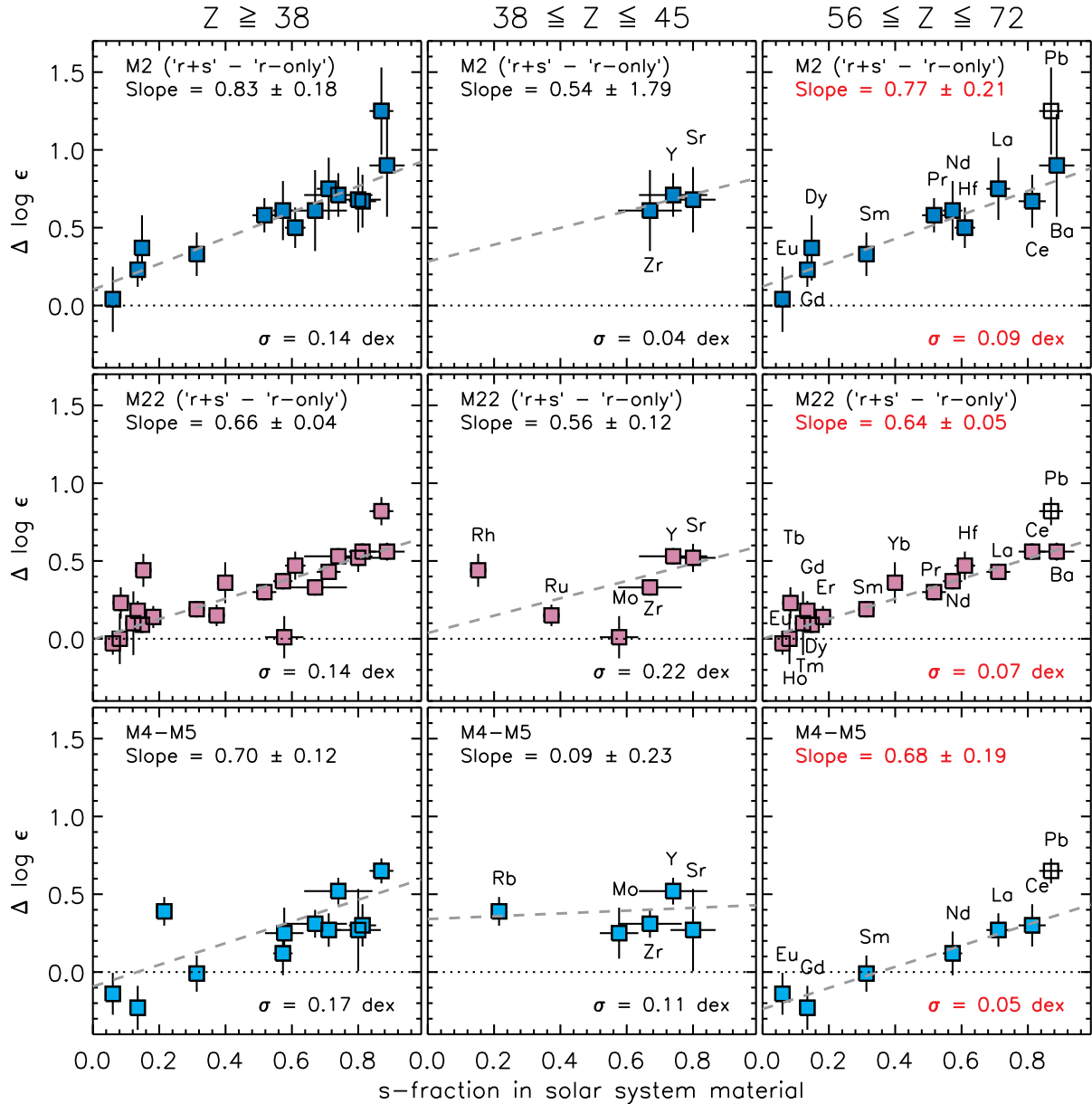


Figure 16. Differences in the mean abundances between the $r+s$ group and the r -only group as a function of the fraction of each element attributed to an s -process origin in solar material (Bisterzo et al. 2011). M2, M22 and M4–M5 are shown in the upper, middle and lower panels, respectively. The elements $Z \geq 38$, $38 \leq Z \leq 45$ and $56 \leq Z \leq 72$ are displayed in the left-hand, middle and right-hand panels, respectively. The dotted line indicates zero difference. In each panel we overplot the linear fit to the data and write the slope and error as well as the dispersion about the fit. In the right panels, we plot Pb ($Z = 82$), although this element is not included in the fit.

posed of independent fragments that experienced different chemical enrichment histories (Searle 1977).

5.3 The origin of the s -process material

If we assume that the r -process enrichment is common to both the r -only and $r+s$ groups in M2, we can subtract the average abundances found in the r -only group from those in the $r+s$ group to obtain the intrinsic abundance ratios of the s -process material added to the $r+s$ group. These differences are shown in Figure 15 (as a function of atomic number) and in Figure 16 (as a function of the fraction of each element attributed to the s -process in solar system material).

Roederer et al. (2011) performed a similar calculation for the two stellar groups in M22 and the unrelated clusters M4 and M5 using data from Yong et al. (2008a,b). In Figure 16, we include the abundance differences for the M22 groups as well as the abundance differences when subtracting the mean values for M5 from those of M4 which we denote as “M4 – M5”¹⁰. In this figure we adopt the values from Bisterzo et al. (2011) for the fraction of each ele-

¹⁰ These are two well-studied unrelated clusters of similar metallicity, $[\text{Fe}/\text{H}] \simeq -1.2$, and M4 is known to exhibit a moderate enhancement in s -process element abundances compared to M5 (Ivans et al. 1999; Ivans et al. 2001). As in Roederer et al. (2011),

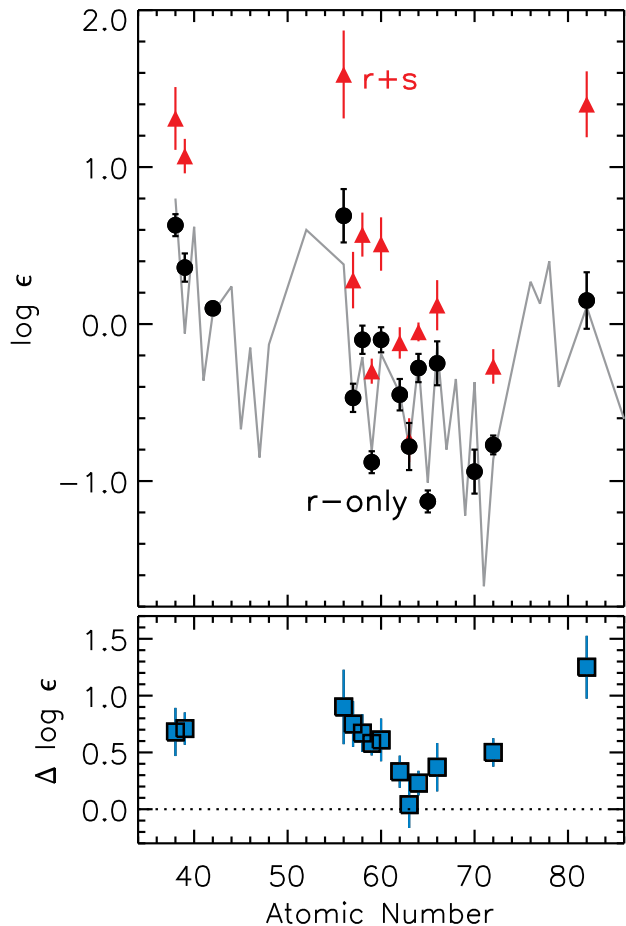


Figure 15. Top panel: Mean logarithmic abundances for the six r -only stars (black circles) and the four $r+s$ stars (red triangles). (Only elements measured in more than one star are included, i.e., we exclude Mo, Er and Tm.) The zirconium abundance derived from Zr II lines is shown. The gray line illustrates the abundances in the r -process standard star BD+17° 3248 normalized to the europium abundance. Bottom panel: Differences in these mean abundances. The dotted line indicates zero difference.

ment attributed to the s -process in solar system material. As noted, there is a clear trend between the abundance differences and the s -process fraction. As originally proposed by Roederer et al. (2011), we argue that the abundance residual represents s -process material.

When considering all elements with $Z \geq 38$ (i.e., Sr and heavier elements), the three “systems,” (1) $\langle r+s \rangle - \langle r \rangle$ in M2, (2) $\langle r+s \rangle - \langle r \rangle$ in M22 and (3) $\langle M4 \rangle - \langle M5 \rangle$, exhibit identical gradients within their mutual uncertainties. Such a result is surprising given that the yields for the s -process elements in AGB stars are mass and metallicity dependent (e.g., Busso et al. 2001; Cristallo et al. 2011; Karakas et al. 2012; Fishlock et al., in preparation). If our interpretation that the abundance residuals in these systems represent s -process material is correct, then the implication is that these three systems, which span a range in metallicity

subtracting the abundances for M5 from M4 attempts to quantify the s -process contribution to M4.

from $[\text{Fe}/\text{H}] \approx -1.8$ to $[\text{Fe}/\text{H}] \approx -1.2$, experienced enrichment by s -process material of indistinguishable composition. Quantitative chemical evolution modelling is needed to test this intriguing hypothesis, and Shingles et al. (in preparation) are investigating M22 and M4 and comparing the predicted and observed enrichment patterns taking into account yields from AGB and massive stars.

If we consider only elements with $38 \leq Z \leq 45$ (i.e., Sr to Rh), the gradients do not exhibit any consistent patterns. In sharp contrast, however, the elements from $56 \leq Z \leq 72$ (i.e., Ba to Hf) exhibit identical gradients within their mutual uncertainties. For these elements, the measured abundance differences in each system are consistent with a single relation. This implies that the enrichment in M2, M22 and M4 involved s -process material of remarkably similar composition despite the factor of ~ 4 difference in metallicity.

The intrinsic s -process ratios and indices¹¹ are $[\text{Pb}/\text{La}]_s = +0.53$ in M2, $+0.18$ in M22 and -0.01 in M4 – M5; $[\text{hs}/\text{ls}]_s = -0.02$ in M2, -0.01 in M22 and -0.50 in M4 – M5; and $[\text{Pb}/\text{hs}]_s = +0.72$ in M2, $+0.29$ in M22 and $+0.28$ in M4 – M5. Uncertainties on these ratios are typically 0.1–0.2 dex. These ratios and indices are largely insensitive to uncertainties in the atomic data and non-LTE effects. For $[\text{Pb}/\text{La}]_s$, M2 exhibits a higher ratio than M22 and M4 – M5. For $[\text{hs}/\text{ls}]_s$, M4 – M5 exhibits lower ratios than M22 and M2, although this may reflect the higher metallicity of M4 and M5 relative to the other two clusters. For $[\text{Pb}/\text{hs}]_s$, M2 exhibits a higher ratio than the other two systems.

A number of studies have investigated s -process nucleosynthesis in metal-poor stars on the AGB (Goriely & Mowlavi 2000; Goriely & Siess 2001; Cristallo et al. 2009, 2011; Bisterzo et al. 2010, Fishlock et al., in preparation). While most of these models fail to offer an exact match for the metallicity of M2, we can use them to get a sense of s -process nucleosynthesis ratios predicted for metallicities higher and lower than M2. We find encouraging agreement when comparing our results to the $[\text{hs}/\text{ls}]_s$ and $[\text{Pb}/\text{hs}]_s$ indices presented in Figures C3 and C5 of Bisterzo et al. (2010) for 3 and 5 M_\odot AGB stars at the appropriate metallicities for M2, M22 and M4 – M5. Furthermore, we note that the yields of Fishlock et al. (in preparation) for their 3 M_\odot and 3.5 M_\odot models for $[\text{Fe}/\text{H}] = -1.2$ bracket the $[\text{Pb}/\text{La}]_s$, $[\text{hs}/\text{ls}]_s$ and $[\text{Pb}/\text{hs}]_s$ ratios in M2, M22 and M4 – M5. Quantitative chemical evolution models based on their yields would be of great interest. Overall, we reach the same conclusion drawn by Roederer et al. (2011): AGB stars with masses less than 3 M_\odot cannot reproduce the observed ratios unless the standard ^{13}C pocket efficiency in the models is reduced by factors of 30 or more.

If we assume that the stars in the $r+s$ group in M2 formed later than the stars in the r -only group, and that the

¹¹ We adopt the indices as defined by Bisterzo et al. (2010): the ratios of light (ls) and heavy (hs) s -process abundances are $[ls/\text{Fe}] \equiv \frac{1}{2}([\text{Y}/\text{Fe}] + [\text{Zr}/\text{Fe}])$ and $[\text{hs}/\text{Fe}] \equiv \frac{1}{3}([\text{La}/\text{Fe}] + [\text{Nd}/\text{Fe}] + [\text{Sm}/\text{Fe}])$. These include elements at the first (Sr, Y, Zr) and second (Ba, La, Ce, Pr, Nd) s -process peaks; Pb is the sole representative of the third s -process peak. Similarly, $[\text{hs}/\text{ls}] \equiv [\text{hs}/\text{Fe}] - [ls/\text{Fe}]$.

AGB stars responsible for distributing this *s*-process material in M2 formed simultaneously with the stars in the *r*-only group, this sets an upper limit on the amount of time that passed between the formation of the *r*-only group and the *r* + *s* group. For a $3 M_{\odot}$ AGB star, adopting the approximate stellar lifetimes computed by Mowlavi et al. (2012), this sets a limit of no more than 300 Myr or so between the two groups. Of course, this limit would be even smaller if higher-mass AGB stars were the source of the *s*-process material. Finally, although we have focused on the neutron-capture elements, the difference in $[\text{Fe}/\text{H}]$ between the *r*-only and *r* + *s* groups requires some source(s) that produces the elements from Si to Zn (and perhaps other elements) to increase the abundances of these elements between these groups.

6 CONCLUSION

In this paper we present a spectroscopic analysis of giant stars in the multiple population globular cluster M2. Our principal and novel results include the following. First, we identify a star-to-star dispersion in iron abundance with the anomalous RGB stars (i.e., stars lying redward of the dominant RGB) being more metal-rich than the canonical RGB objects. The iron abundance distribution has a dominant peak at $[\text{Fe}/\text{H}] \approx -1.7$ and smaller peaks at -1.5 and -1.0 , although membership for the latter group remains to be established. Secondly, the neutron-capture element abundances exhibit a star-to-star dispersion with a possible bimodal distribution. In this regard, M2 is chemically similar to the globular clusters M22, NGC 1851 and ω Cen, whose subgiant branches exhibit multiple sequences. It is likely that M2 has therefore experienced a similarly complex formation history. Thirdly, when subtracting the average abundances in the *r*-only group from those of the *r* + *s* group, the abundance residual exhibits a striking correlation with the fraction of each element attributed to the *s*-process in solar system material. This residual is remarkably similar to that found in M22 and in M4 – M5. Such a similarity would indicate that M2, M22, and M4 were enriched by *s*-process material of identical composition and potentially offers important observational constraints on the nature of the *s*-process in low metallicity environments. A comparison with theoretical predictions reveals that AGB stars with masses less than $3 M_{\odot}$ are unlikely to have played a major role in the chemical enrichment of M2. In addition to the AGB star contribution, some source(s) is needed to increase the abundances of the elements from Si to Zn in the *r* + *s* group relative to the *r*-only group. Additional studies are essential to understand the formation and evolution of this complex cluster.

ACKNOWLEDGMENTS

We thank K. Cudworth for providing electronic data and the referee, Kim Venn, for helpful comments. Some of the AAT data were taken in time allocated to the AEGIS program (PI Keller). The authors are grateful to the AEGIS team for access to these data. D.Y, G.D.C, A.I.K, J.E.N, A.F.M

and A.P.M gratefully acknowledge support from the Australian Research Council (grants DP0984924, FT110100475, DP120100475, DP120100991 and DP120101237). Funding for the Stellar Astrophysics Centre is provided by The Danish National Research Foundation. The research is supported by the ASTERISK project (ASTERoseismic Investigations with SONG and Kepler) funded by the European Research Council (Grant agreement no.: 267864).

REFERENCES

- Allende Prieto, C., Barklem, P. S., Lambert, D. L., & Cunha, K. 2004, *A&A*, 420, 183
- Alonso, A., Arribas, S., & Martínez-Roger, C. 1999, *A&AS*, 140, 261
- Armandroff, T. E. & Da Costa, G. S. 1991, *AJ*, 101, 1329
- Armandroff, T. E. & Zinn, R. 1988, *AJ*, 96, 92
- Arp, H. C. 1955, *AJ*, 60, 317
- Asplund, M., Grevesse, N., Sauval, A. J., & Scott, P. 2009, *ARA&A*, 47, 481
- Bedin, L. R., Piotto, G., Anderson, J., Cassisi, S., King, I. R., Momany, Y., & Carraro, G. 2004, *ApJ*, 605, L125
- Bekki, K. 2011, *MNRAS*, 412, 2241
- Bekki, K. & Freeman, K. C. 2003, *MNRAS*, 346, L11
- Bekki, K. & Yong, D. 2012, *MNRAS*, 419, 2063
- Bergemann, M., Hansen, C. J., Bautista, M., & Ruchti, G. 2012, *A&A*, 546, A90
- Bernstein, R., Sheckman, S. A., Gunnels, S. M., Mochnacki, S., & Athey, A. E. 2003, in *Society of Photo-Optical Instrumentation Engineers (SPIE) Conference Series*, Vol. 4841, *Society of Photo-Optical Instrumentation Engineers (SPIE) Conference Series*, ed. M. Iye & A. F. M. Moorwood, 1694–1704
- Biemont, E., Baudoux, M., Kurucz, R. L., Ansbacher, W., & Pinnington, E. H. 1991, *A&A*, 249, 539
- Biémont, É., Blagoev, K., Engström, L., Hartman, H., Lundberg, H., Malcheva, G., Nilsson, H., Whitehead, R. B., Palmeri, P., & Quinet, P. 2011, *MNRAS*, 414, 3350
- Biémont, E., Garnir, H. P., Palmeri, P., Li, Z. S., & Svanberg, S. 2000, *MNRAS*, 312, 116
- Biemont, E., Grevesse, N., Hannaford, P., & Lowe, R. M. 1981, *ApJ*, 248, 867
- Bisterzo, S., Gallino, R., Straniero, O., Cristallo, S., & Käppeler, F. 2010, *MNRAS*, 404, 1529
- . 2011, *MNRAS*, 418, 284
- Blackwell, D. E., Booth, A. J., Haddock, D. J., Petford, A. D., & Leggett, S. K. 1986, *MNRAS*, 220, 549
- Blackwell, D. E., Ibbetson, P. A., Petford, A. D., & Shallis, M. J. 1979a, *MNRAS*, 186, 633
- Blackwell, D. E., Lynas-Gray, A. E., & Smith, G. 1995, *A&A*, 296, 217
- Blackwell, D. E., Petford, A. D., & Shallis, M. J. 1979b, *MNRAS*, 186, 657
- Blackwell, D. E., Petford, A. D., Shallis, M. J., & Simmons, G. J. 1980, *MNRAS*, 191, 445
- Busso, M., Gallino, R., Lambert, D. L., Travaglio, C., & Smith, V. V. 2001, *ApJ*, 557, 802
- Carretta, E., Bragaglia, A., Gratton, R., D’Orazi, V., & Lucatello, S. 2009, *A&A*, 508, 695
- Carretta, E., Bragaglia, A., Gratton, R. G., D’Orazi, V., Lucatello, S., Momany, Y., Sollima, A., Bel-

- lazzini, M., Catanzaro, G., & Leone, F. 2014, *A&A* in press (arXiv:1401.7325)
- Carretta, E., Bragaglia, A., Gratton, R. G., Lucatello, S., Bellazzini, M., Catanzaro, G., Leone, F., Momany, Y., Piotto, G., & D’Orazi, V. 2010a, *A&A*, 520, A95
- . 2010b, *ApJ*, 714, L7
- Carretta, E., Bragaglia, A., Gratton, R. G., Lucatello, S., D’Orazi, V., Bellazzini, M., Catanzaro, G., Leone, F., Momany, Y., & Sollima, A. 2013, *A&A*, 557, A138
- Carretta, E., Gratton, R. G., Lucatello, S., Bragaglia, A., Catanzaro, G., Leone, F., Momany, Y., D’Orazi, V., Cassisi, S., D’Antona, F., & Ortolani, S. 2010c, *ApJ*, 722, L1
- Carretta, E., Lucatello, S., Gratton, R. G., Bragaglia, A., & D’Orazi, V. 2011, *A&A*, 533, A69
- Castelli, F. & Kurucz, R. L. 2003, in *IAU Symp. 210, Modelling of Stellar Atmospheres*, ed. N. Piskunov, W. W. Weiss, & D. F. Gray (San Francisco, CA: ASP), A20
- Conroy, C. & Spergel, D. N. 2011, *ApJ*, 726, 36
- Cowan, J. J., Sneden, C., Beers, T. C., Lawler, J. E., Simmerer, J., Truran, J. W., Primas, F., Collier, J., & Burles, S. 2005, *ApJ*, 627, 238
- Cowan, J. J., Sneden, C., Burles, S., Ivans, I. I., Beers, T. C., Truran, J. W., Lawler, J. E., Primas, F., Fuller, G. M., Pfeiffer, B., & Kratz, K.-L. 2002, *ApJ*, 572, 861
- Cristallo, S., Piersanti, L., Straniero, O., Gallino, R., Domínguez, I., Abia, C., Di Rico, G., Quintini, M., & Bisterzo, S. 2011, *ApJS*, 197, 17
- Cristallo, S., Straniero, O., Gallino, R., Piersanti, L., Domínguez, I., & Lederer, M. T. 2009, *ApJ*, 696, 797
- Cudworth, K. M. & Rauscher, B. J. 1987, *AJ*, 93, 856
- Cunha, K., Smith, V. V., Suntzeff, N. B., Norris, J. E., Da Costa, G. S., & Plez, B. 2002, *AJ*, 124, 379
- Da Costa, G. S., Held, E. V., & Saviane, I. 2014, *MNRAS*, 438, 3507
- Da Costa, G. S., Held, E. V., Saviane, I., & Gullieuszik, M. 2009, *ApJ*, 705, 1481
- D’Antona, F., Ventura, P., Caloi, V., D’Ercole, A., Vesperini, E., Carini, R., & Di Criscienzo, M. 2010, *ApJ*, 715, L63
- de Mink, S. E., Pols, O. R., Langer, N., & Izzard, R. G. 2009, *A&A*, 507, L1
- Decressin, T., Meynet, G., Charbonnel, C., Prantzos, N., & Ekström, S. 2007, *A&A*, 464, 1029
- Den Hartog, E. A., Lawler, J. E., Sneden, C., & Cowan, J. J. 2003, *ApJS*, 148, 543
- . 2006, *ApJS*, 167, 292
- D’Ercole, A., Vesperini, E., D’Antona, F., McMillan, S. L. W., & Recchi, S. 2008, *MNRAS*, 391, 825
- D’Orazi, V., Gratton, R. G., Pancino, E., Bragaglia, A., Carretta, E., Lucatello, S., & Sneden, C. 2011, *A&A*, 534, A29
- Dotter, A., Chaboyer, B., Jevremović, D., Kostov, V., Baron, E., & Ferguson, J. W. 2008, *ApJS*, 178, 89
- Fenner, Y., Campbell, S., Karakas, A. I., Lattanzio, J. C., & Gibson, B. K. 2004, *MNRAS*, 353, 789
- Fuhr, J. R. & Wiese, W. L. 2009, in *CRC Handbook of Chemistry and Physics*, 90th edn. CRC Press, Boca Raton, p. 10
- Fulbright, J. P. 2000, *AJ*, 120, 1841
- Girardi, L., Groenewegen, M. A. T., Hatziminaoglou, E., & da Costa, L. 2005, *A&A*, 436, 895
- Goriely, S. & Mowlavi, N. 2000, *A&A*, 362, 599
- Goriely, S. & Siess, L. 2001, *A&A*, 378, L25
- Gratton, R., Sneden, C., & Carretta, E. 2004, *ARA&A*, 42, 385
- Gratton, R. G., Carretta, E., & Bragaglia, A. 2012, *A&A Rev.*, 20, 50
- Gratton, R. G., Carretta, E., Claudi, R., Lucatello, S., & Barbieri, M. 2003, *A&A*, 404, 187
- Grundahl, F., Catelan, M., Landsman, W. B., Stetson, P. B., & Andersen, M. I. 1999, *ApJ*, 524, 242
- Hansen, C. J., Bergemann, M., Cescutti, G., François, P., Arcones, A., Karakas, A. I., Lind, K., & Chiappini, C. 2013, *A&A*, 551, A57
- Harris, W. E. 1975, *ApJS*, 29, 397
- . 1996, *AJ*, 112, 1487
- Herwig, F., Vandenberg, D. A., Navarro, J. F., Ferguson, J., & Paxton, B. 2012, *ApJ*, 757, 132
- Ivans, I. I., Kraft, R. P., Sneden, C., Smith, G. H., Rich, R. M., & Shetrone, M. 2001, *AJ*, 122, 1438
- Ivans, I. I., Simmerer, J., Sneden, C., Lawler, J. E., Cowan, J. J., Gallino, R., & Bisterzo, S. 2006, *ApJ*, 645, 613
- Ivans, I. I., Sneden, C., Kraft, R. P., et al. 1999, *AJ*, 118, 1273
- Ivarsson, S., Litzén, U., & Wahlgren, G. M. 2001, *Phys. Scr*, 64, 455
- Johnson, C. I. & Pilachowski, C. A. 2010, *ApJ*, 722, 1373
- Karakas, A. I., García-Hernández, D. A., & Lugaro, M. 2012, *ApJ*, 751, 8
- Kraft, R. P. 1994, *PASP*, 106, 553
- Kurucz, R. & Bell, B. 1995, *Atomic Line Data* (R.L. Kurucz and B. Bell) Kurucz CD-ROM No. 23. Cambridge, Mass.: Smithsonian Astrophysical Observatory, 1995., 23
- Lardo, C., Pancino, E., Mucciarelli, A., Bellazzini, M., Rejkuba, M., Marinoni, S., Cocozza, G., Altavilla, G., & Ragaini, S. 2013, *MNRAS*, 433, 1941
- Lardo, C., Pancino, E., Mucciarelli, A., & Milone, A. P. 2012, *A&A*, 548, A107
- Lawler, J. E., Bonvallet, G., & Sneden, C. 2001a, *ApJ*, 556, 452
- Lawler, J. E., den Hartog, E. A., Labby, Z. E., Sneden, C., Cowan, J. J., & Ivans, I. I. 2007, *ApJS*, 169, 120
- Lawler, J. E., Den Hartog, E. A., Sneden, C., & Cowan, J. J. 2006, *ApJS*, 162, 227
- Lawler, J. E., Sneden, C., Cowan, J. J., Ivans, I. I., & Den Hartog, E. A. 2009, *ApJS*, 182, 51
- Lawler, J. E., Sneden, C., Cowan, J. J., Wyart, J.-F., Ivans, I. I., Sobeck, J. S., Stockett, M. H., & Den Hartog, E. A. 2008, *ApJS*, 178, 71
- Lawler, J. E., Wickliffe, M. E., Cowley, C. R., & Sneden, C. 2001b, *ApJS*, 137, 341
- Lawler, J. E., Wickliffe, M. E., den Hartog, E. A., & Sneden, C. 2001c, *ApJ*, 563, 1075
- Lawler, J. E., Wyart, J.-F., & Blaise, J. 2001d, *ApJS*, 137, 351
- Li, R., Chatelain, R., Holt, R. A., Rehse, S. J., Rosner, S. D., & Scholl, T. J. 2007, *Phys. Scr*, 76, 577
- Ljung, G., Nilsson, H., Asplund, M., & Johansson, S. 2006, *A&A*, 456, 1181
- Marcolini, A., Sollima, A., D’Ercole, A., Gibson, B. K., & Ferraro, F. R. 2007, *MNRAS*, 382, 443
- Marino, A. F., Milone, A. P., Piotto, G., Villanova, S., Bedin, L. R., Bellini, A., & Renzini, A. 2009, *A&A*, 505, 1099

- Marino, A. F., Sneden, C., Kraft, R. P., Wallerstein, G., Norris, J. E., da Costa, G., Milone, A. P., Ivans, I. I., Gonzalez, G., Fulbright, J. P., Hilker, M., Piotto, G., Zoccali, M., & Stetson, P. B. 2011, *A&A*, 532, A8
- Mashonkina, L., Ryabtsev, A., & Frebel, A. 2012, *A&A*, 540, A98
- McWilliam, A. 1998, *AJ*, 115, 1640
- Milone, A. P., Bedin, L. R., Piotto, G., Anderson, J., King, I. R., Sarajedini, A., Dotter, A., Chaboyer, B., Marín-Franch, A., Majewski, S., Aparicio, A., Hempel, M., Paust, N. E. Q., Reid, I. N., Rosenberg, A., & Siegel, M. 2008, *ApJ*, 673, 241
- Mishenina, T. V., Kovtyukh, V. V., Soubiran, C., Travaglio, C., & Busso, M. 2002, *A&A*, 396, 189
- Mowlavi, N., Eggenberger, P., Meynet, G., Ekström, S., Georgy, C., Maeder, A., Charbonnel, C., & Eyer, L. 2012, *A&A*, 541, A41
- Noguchi, K., Aoki, W., Kawanomoto, S., Ando, H., Honda, S., Izumiura, H., Kambe, E., Okita, K., Sadakane, K., Sato, B., Tajitsu, A., Takada-Hidai, T., Tanaka, W., Watanabe, E., & Yoshida, M. 2002, *PASJ*, 54, 855
- Norris, J. E. & Da Costa, G. S. 1995a, *ApJ*, 447, 680
- . 1995b, *ApJ*, 441, L81
- Otsuki, K., Honda, S., Aoki, W., Kajino, T., & Mathews, G. J. 2006, *ApJ*, 641, L117
- Pancino, E., Pasquini, L., Hill, V., Ferraro, F. R., & Bellazzini, M. 2002, *ApJ*, 568, L101
- Piotto, G. 2009, in *IAU Symposium*, Vol. 258, *IAU Symposium*, ed. E. E. Mamajek, D. R. Soderblom, & R. F. G. Wyse, 233–244
- Piotto, G., Milone, A. P., Anderson, J., Bedin, L. R., Bellini, A., Cassisi, S., Marino, A. F., Aparicio, A., & Nascimbeni, V. 2012, *ApJ*, 760, 39
- Primas, F. & Sobeck, J. 2008, in *American Institute of Physics Conference Series*, Vol. 1001, *Evolution and Nucleosynthesis in AGB Stars*, ed. R. Guandalini, S. Palmerini, & M. Busso, 230–234
- Prochaska, J. X., Naumov, S. O., Carney, B. W., McWilliam, A., & Wolfe, A. M. 2000, *AJ*, 120, 2513
- Ramírez, I. & Meléndez, J. 2005, *ApJ*, 626, 465
- Ramírez, S. V. & Cohen, J. G. 2002, *AJ*, 123, 3277
- Robin, A. C., Reylé, C., Derrière, S., & Picaud, S. 2003, *A&A*, 409, 523
- Roederer, I. U., Cowan, J. J., Karakas, A. I., Kratz, K.-L., Lugaro, M., Simmerer, J., Farouqi, K., & Sneden, C. 2010a, *ApJ*, 724, 975
- Roederer, I. U. & Lawler, J. E. 2012, *ApJ*, 750, 76
- Roederer, I. U., Lawler, J. E., Cowan, J. J., Beers, T. C., Frebel, A., Ivans, I. I., Schatz, H., Sobeck, J. S., & Sneden, C. 2012a, *ApJ*, 747, L8
- Roederer, I. U., Lawler, J. E., Sneden, C., Cowan, J. J., Sobeck, J. S., & Pilachowski, C. A. 2008, *ApJ*, 675, 723
- Roederer, I. U., Lawler, J. E., Sobeck, J. S., Beers, T. C., Cowan, J. J., Frebel, A., Ivans, I. I., Schatz, H., Sneden, C., & Thompson, I. B. 2012b, *ApJS*, 203, 27
- Roederer, I. U., Marino, A. F., & Sneden, C. 2011, *ApJ*, 742, 37
- Roederer, I. U., Sneden, C., Lawler, J. E., & Cowan, J. J. 2010b, *ApJ*, 714, L123
- Romano, D. & Matteucci, F. 2007, *MNRAS*, 378, L59
- Saunders, W., Bridges, T., Gillingham, P., Haynes, R., Smith, G. A., Whittard, J. D., Churilov, V., Lankshear, A., Croom, S., Jones, D., & Boshuizen, C. 2004, in *Society of Photo-Optical Instrumentation Engineers (SPIE) Conference Series*, Vol. 5492, *Society of Photo-Optical Instrumentation Engineers (SPIE) Conference Series*, ed. A. F. M. Moorwood & M. Iye, 389–400
- Saviane, I., da Costa, G. S., Held, E. V., Sommariva, V., Gullieuszik, M., Barbuy, B., & Ortolani, S. 2012, *A&A*, 540, A27
- Searle, L. 1977, in *Evolution of Galaxies and Stellar Populations*, ed. B. M. Tinsley & R. B. G. Larson, D. Campbell, 219
- Simmerer, J., Sneden, C., Ivans, I. I., Kraft, R. P., Shetrone, M. D., & Smith, V. V. 2003, *AJ*, 125, 2018
- Skrutskie, M. F., Cutri, R. M., Stiening, R., Weinberg, M. D., Schneider, S., Carpenter, J. M., Beichman, C., Capps, R., Chester, T., Elias, J., Huchra, J., Liebert, J., Lonsdale, C., Monet, D. G., Price, S., Seitzer, P., Jarrett, T., Kirkpatrick, J. D., Gizis, J. E., Howard, E., Evans, T., Fowler, J., Fullmer, L., Hurt, R., Light, R., Kopan, E. L., Marsh, K. A., McCallon, H. L., Tam, R., Van Dyk, S., & Wheelock, S. 2006, *AJ*, 131, 1163
- Smith, G. H. 1987, *PASP*, 99, 67
- Smith, G. H. & Mateo, M. 1990, *ApJ*, 353, 533
- Smith, V. V., Suntzeff, N. B., Cunha, K., Gallino, R., Busso, M., Lambert, D. L., & Straniero, O. 2000, *AJ*, 119, 1239
- Smolinski, J. P., Martell, S. L., Beers, T. C., & Lee, Y. S. 2011, *AJ*, 142, 126
- Sneden, C. 1973, *ApJ*, 184, 839
- Sneden, C. & Crocker, D. A. 1988, *ApJ*, 335, 406
- Sneden, C., Johnson, J., Kraft, R. P., Smith, G. H., Cowan, J. J., & Bolte, M. S. 2000, *ApJ*, 536, L85
- Sneden, C., Kraft, R. P., Shetrone, M. D., Smith, G. H., Langer, G. E., & Prosser, C. F. 1997, *AJ*, 114, 1964
- Sneden, C., Lawler, J. E., Cowan, J. J., Ivans, I. I., & Den Hartog, E. A. 2009, *ApJS*, 182, 80
- Sobeck, J. S., Kraft, R. P., Sneden, C., Preston, G. W., Cowan, J. J., Smith, G. H., Thompson, I. B., Shectman, S. A., & Burley, G. S. 2011, *AJ*, 141, 175
- Stetson, P. B. & Pancino, E. 2008, *PASP*, 120, 1332
- Ventura, P. & D’Antona, F. 2005, *ApJ*, 635, L149
- Vesperini, E., McMillan, S. L. W., D’Antona, F., & D’Ercole, A. 2013, *MNRAS*, 429, 1913
- Villanova, S., Piotto, G., & Gratton, R. G. 2009, *A&A*, 499, 755
- Whaling, W. & Brault, J. W. 1988, *Phys. Scr*, 38, 707
- Wickliffe, M. E. & Lawler, J. E. 1997, *ApJS*, 110, 163
- Wickliffe, M. E., Lawler, J. E., & Nave, G. 2000, *J. Quant. Spec. Radiat. Transf.*, 66, 363
- Worley, C. C., Hill, V., Sobeck, J., & Carretta, E. 2013, *A&A*, 553, A47
- Yong, D., Aoki, W., Lambert, D. L., & Paulson, D. B. 2006, *ApJ*, 639, 918
- Yong, D. & Grundahl, F. 2008, *ApJ*, 672, L29
- Yong, D., Grundahl, F., Nissen, P. E., Jensen, H. R., & Lambert, D. L. 2005, *A&A*, 438, 875
- Yong, D., Karakas, A. I., Lambert, D. L., Chieffi, A., & Limongi, M. 2008a, *ApJ*, 689, 1031
- Yong, D., Lambert, D. L., Paulson, D. B., & Carney, B. W. 2008b, *ApJ*, 673, 854